

## Response to reviewer #1

We first would like to sincerely thank the reviewer for his throughout review and his numerous useful comments that, we believe, contribute to significantly improve our manuscript. Each answer/comment of the reviewer below is followed by a “response” and when applicable by a more specific description of the “change(s)” we made to the manuscript.

### General comment 1:

**“Determining the deformation of a material element using a finite set of discreet points leads to a “boundary definition” error for the line integral that increases as the number of points decreases. The RGPS data set uses four-point cells to compute the deformation. The method proposed here starts with just three points, the minimum possible and the configuration with the maximum error. Thorndike 1986) discusses how the number of nodes determines the accuracy of the deformation estimates. Three nodes are worse than four by a factor of 2 or 3 (his Figure 23b).”**

**Thorndike, A. S. (1986), Kinematics of Sea Ice, in The Geophysics of Sea Ice, NATO ASI Series, edited by N. Untersteiner, Plenum Press, New York, pp 489-549.**

#### Response:

This comment helped us to better characterize the accuracy of the unfiltered deformation obtained when using three or four nodes. We can now state that the error due to spurious opening/closing when using triangles is about 10% higher than the error obtained when using quadrangles. This new analysis is presented hereafter and in the paper.

We also discuss hereafter why the analysis of Thorndike (1986) and the statement: “Three nodes are worse than four by a factor of 2 or 3” do not apply to our problem.

Lindsay and Stern (2003) specifically studied the relationship between the number of points taken to compute deformation and the error due to spurious opening/closing. They found that the error drops by almost 50% when using 8 points instead of 4 points. When using 4 points (quadrangles), Lindsay and Stern (2003) found an error of 15% of the sliding distance. In the original manuscript, we presented the same kind of analysis with a simple test case considering one single crack. We found an error equal to 20% of the sliding distance when using 3 points (triangles).

We have now also analyzed the single crack test case when using quadrangles and we found that the opening/closing error is about 18% of the sliding distance. The opening/closing error when using triangles (3 points) is then only about 10% higher than the error obtained with quadrangles (4 points).

The factor of 10% found for the opening/closing errors is actually not in contradiction with the factor 2 or 3 derived from the analysis of Thorndike (1986) as the analyzed problems are actually not the same. The analysis of Thorndike (1986) estimates the “boundary definition” error over a circular region as a function of the number measurements on the circumference of this region. The error is then only estimated on the mean deformation over this region and does not take into account the spurious opening and closing that could occurs within this region. In our analysis, we also define a region (here a square domain) but we do not only consider the measurements at the circumference but all the measurements available at a given resolution within this region. In our case, the error is not estimated on the mean deformation over the region but as the accumulation of error for each cell.

For more details on the single crack test case with quadrangles, see our answer to the remark on Figure1.

We also add more justification on the choice of using triangles (See response to the remark of reviewer#2 related to Page 5113 lines 18-19).

Changes:

We add this paragraph:

“When repeating the same test case with quadrangles instead of triangles, we found a rms error of about 18% of the sliding distance  $u_p$ . For comparison, Lindsay (2003) found an error per unit crack of about 15 % of the sliding distance, for a similar test case on a mesh made of square cells. This analysis shows that using triangles only generates an increase of about 10 % of the opening (and closing) error compare to using quadrangles. This increase of the error is minor compared to the advantages of using triangles. Triangulation methods are more flexible. It roughly doubles the number of deformation estimates and it increases the resolution at which deformation is defined. For the rest of this paper, we then only present results on triangular meshes but the method could also be applied to other type of meshes.”

**General comment 2:**

**“1) The spatial scale of the filtered data is ambiguous because the deformation is smoothed with between 1 to 10 or more triangles, so what is the spatial scale of each observation in the smoothed data? 2) How is the spatial scale determined for the scaling analysis? 3) The smoothing procedure has reduced the noise at the expense of spatial scale, as must always be the case with discrete points for the velocity. 4) Can the authors please more fully explore these ideas in the introduction?”**

Response:

1) We agree that with a classical smoother the spatial scale of the smoothed deformation field does not have the same spatial scale as the unfiltered deformation field. For example, we found in the case of a unique crack that the value of the filtered shear along the crack is inversely proportional to  $n$ . This indicates that classical smoothers modify the spatial scale at which the deformation is defined. However, our method is different than classical smoothers. As explained in the manuscript, our method is “based on the fact that the deformation is by nature constant along a linear kinematic feature. Averaging motion derivatives along these features could then filter out the noise without spoiling the information on the real deformation.” We verified this hypothesis with the single crack test case and we found that with our method the shear along the crack does not vary as a function of  $n$ , meaning that with our method the spatial scale of each observation in the smoothed data is the same as in the unfiltered data.

2) The spatial scale is the square root of the sum of the areas of the cells selected by the coarse graining procedure. See also our response to remark 5116-21.

3) We do not agree. In the case of the single crack, deformation should be constant along the crack but is polluted by the artificial noise. Averaging the deformation over the elements crossed by the crack should then not change the mean value of the deformation but only reduces the noise. In other words, whatever is the number of triangles used for the average, the spatial scale remains the same.

4) We now discuss these ideas and the difference between classical smoothers and our method in the presentation of the method.

Changes:

1) We add the following sentences in the paragraph presenting the classical smoother: “It also modifies the spatial scale at which the deformation is defined, resulting in a modification of the value of the shear along the crack. With the single crack case, the area-weighted average of the shear for the cells cut by the crack is found to be inversely proportional to  $n$ ”.

We add the following sentences when presenting our method: “Contrary to the smoother presented here above, the scale at which the deformation is defined remains constant with the second method. In other words, the mean value of the shear along the crack obtained with the second method does not vary as a function of  $n$ . We also verified that in the case of a regular mesh and a single crack aligned with the  $x$ -axis, the area-weighted average of the shear along the crack is strictly constant whatever the value of  $n$ .”

2) More explanation on the scaling analysis has been added in the text. See our response to remark 5116-21.

3) No changes.

4) We now discuss the difference between classical smoothers and our method in the presentation of the method (see changes 1) here above).

**Specific comments:**

**5106-2: Your method is far from nearly noise free.**

Response: We agree that this statement is not very clear as we haven't quantified the remaining noise.

Changes: new sentence: "We propose a method to reduce the error generated when computing sea ice deformation fields from SAR-derived sea ice motion."

**5106-17: Please give the original references for the cross-correlation techniques applied to SAR images.**

Response: We added the references proposed by Referee #2: Fily and Rothrock (JGR-Oceans 1990) and Kwok et al (IEEE J. Ocean Engr 1990).

Changes: References added

**5106-20: Also maybe reference GlobICE here.**

Response: This is a good suggestion but as far as we know, there is no peer-reviewed publication that we could use to make reference to the GlobICE dataset. Any suggestion would be welcome if we have missed a reference. For now, we therefore do not to add any reference to GlobICE in the introduction section.

Changes: No change

**5107-27: What fraction of the RGPS deformation estimates is afflicted with this problem? Does it change the scaling analysis? How big a problem is this and can unrealistic values be easily filtered out? This seems to be one of your main motivations, but you have not really shown it to be a big problem.**

Response: A very small fraction of the dataset is polluted by these unrealistic values, however it has a high impact on the scaling but also on the total opening and closing when integrated over the Arctic basin. The multifractal scaling analysis is very sensitive to extreme values, particularly when looking at the highest moment orders of the distributions. This is why in some studies based on RGPS deformation dataset the extreme values were simply eliminated with a threshold on the total deformation. However using such a threshold may also eliminate real extreme values. In other studies, the presence and impacts of these extreme values are simply not discussed. From the RGPS deformation dataset, it is not possible to know exactly what is the current shape of the quadrangles used to compute the deformation, it is then not possible to eliminate all the badly shaped element. Our approach based on the definition of a new mesh from the actual position of the RGPS data eliminates this problem.

Changes:

We modified the discussion on the presence of extremes values to answer these questions.

"For the period 2--10~February 2007, the composite picture made from RGPS has maximum opening, closing and shear rates equal to 1.73, -6.73 and 66.47 per day, respectively. These extreme values arise from highly distorted cells. A very small fraction of the dataset is polluted by these unrealistic values, however it has a high impact on the multifractal scaling analysis, particularly when looking at the highest moment orders of the distributions. In Marsan (2004) and Stern (2009), additional constraints on the initial and current size of the cells were applied and the cells with total deformation higher than 1 per day were not taken into account. In many other studies based on the RGPS deformation dataset, the presence and impacts of these unrealistic extreme values are simply not discussed.

The simple fact of redefining a new mesh from the actual position of the RGPS nodes allows us to avoid badly shaped cells and then to significantly reduce the number and magnitude of extreme values. For the same period, the composite picture obtained from the unfiltered version of our RGPS Image Pair dataset has maximum opening, closing and shear rates equal to 0.63, -1.17 and 1.97 per day, respectively. The smoother also logically decreases the extreme values. For this example, the filtered composite picture has maximum opening, closing and shear rates equal to 0.13, -0.20 and 0.73 per day, respectively."

**5108-1: It would be useful here to elaborate on the difficulty in determining the line integral of the velocity for a material element (a cell) using a finite number of points. This might be a good place to have a complete discussion of the ideas presented by Thorndike (1986) about the error of deformation estimates due to the boundary definition and the number of points used.**

Response: As explained in the answer to the general comment 1, the analysis made in Thorndike (1986) does not correspond to the problem we are trying to solve.

Changes: No change

**5110-14: experience → experiment**

Response: Thank you for the correction.

Changes: This change has been applied at 3 different locations in the text.

**5110-20: What is “normalized resolution”?**

Response: It is the mean distance between the points used for the “simple” test-cases. It is called normalized resolution as it is defined for a normalized area equal to 1 and should not be confounded with the resolution of the meshes generated to treat the actual observations.

Changes: We have now added this sentence to the first paragraph of section 2.1: “d is hereafter called the normalized resolution.”

**5110-8: What becomes of the cells below the threshold? Is the filtering applied to these?**

Response: The filtering does not apply to the cells whose deformation is below the threshold.

Changes: We add the following sentence for clarification: “No filtering is applied on the cells where deformation is below the threshold.”

**5111-4: 1) What is the equation for performing the smoothing? 2) Are the tensor components smoothed or just the invariants? 3) Exactly how are the kernel triangles selected? For example, are triangles included if there are no others above the threshold between a kernel triangle and the target triangle? (e.g. if there is a gap in the total deformation). 4) Are all target triangles smoothed, even if they are below the threshold? 5) For example if a triangle is near but not part of an LKF, is the smoother applied to it as well? 6) Or if it is part of the LKF, but below the threshold, is the smoother applied? 7) How would the two cases be distinguished?**

Response:

1) The equation is now given in the text.

2) As explained in the original text (page 6, lines 25-26), the tensor components are smoothed. We agree with the reviewer that the equation makes it now clearer.

3) The kernel around a given reference cell is built as the subset of cells that fulfill the threshold criterion on the total deformation rate, and that can be reached from that reference cell by crossing a maximum of n successive edges.

4-5-6-7 The triangles below the threshold are not smoothed.

Changes:

We changed two paragraphs to answer these questions and to clarify the smoothing methods:

“We here denoted  $C$  the list of all the cells and for each cell  $c \in C$ , we define the kernel  $K_c \subset C$  as the subset of cells that can be reached by crossing a maximum of  $n$  edges. An example of kernel with  $n=7$  is shown in Fig1c and d. The size of the kernel is noted  $|K_c|$ . For the example shown in Fig1c and d,  $|K_c|$  is equal to 87. The components of the filtered deformation are then defined by averaging over the cells of the kernel. For example, the filtered value for  $u_x$  on the cell  $c$  is defined as  $\tilde{u}_x^c = 1/|K_c| \sum_{k \in K_c} u^k_x$ .”

“We denoted  $S$  the list of all the selected cells. For each cell  $s \in S$ , we define the kernel  $K_s \subset S$  as the subset of cells that can be reached by crossing only selected cells and a maximum of  $n$  edges. No filtering is applied on the cells where deformation is below the threshold. Our method preserves the localization of the deformation by avoiding mixing the deformation between LKFs (i.e., cells where the deformation is intense) and the surrounding

rigid plates (i.e., cells where deformation is almost zero). Moreover, the way the smoothing kernels are built ensures that deformation between LKFs that are not connected will not be averaged together.”

**5111-11: Can you show that your smoother is unbiased? The mean divergence along the crack should be zero for both the unfiltered and the smoothed data and the mean shear should be the same for both. Does the thresholding method introduce a bias? You may need to use a much longer crack.**

Response: On average the smoothing method does not introduce any bias. It was already shown in the conclusion of the paper when we said that the cumulative opening and closing are both reduced by the same value of about 60% when comparing the filtered data to the unfiltered one for the whole winter 2006-2007.

For one particular crack, the mean divergence and shear are not exactly the same in the unfiltered and smoothed data. For example, in the case of a single crack aligned with the x-axis, the mean divergence over the square domain in the unfiltered data is exactly zero when the mean divergence in the smoothed data only tends to zero for large  $n$ . However this error in the mean divergence of the smoothed data is always about one order of magnitude smaller than the error on the total opening/closing error of the unfiltered data. Moreover, when looking at a large number of single crack experiments, we verified that this error equally corresponds to negative or positive mean divergence, meaning that the mean divergence over a large number of cracks will not be influenced by this error. Concerning the threshold, it cannot introduce a bias as the threshold is on the total deformation, which is independent of the sign of the divergence.

Changes: No changes have been made to the text.

**5111-19: The line with the disks in Fig.2 seems to go down to 5 or 6%, not 10%. What is the “residual error”?**

Response: You are right. This was a mistake in the text, the residual error is about 5%, not 10%. The residual error is defined as the error remaining for large value of  $n$ .

Changes: We correct the value given in the text and we add this clarification for the residual error:

“For a resolution of 0.1, the residual error (i.e., the error remaining for  $n > d^{-1}$ ) is about 5% as shown in Fig. 2.”

**5113-1: RGPS updates a cell only when all four points are simultaneously updated. There is no asynchronous error.**

Response: We acknowledge our mistake due to a wrong interpretation regarding the synchronicity of the data in the RGPS deformation dataset.

Changes: We removed the statements related to asynchronous error.

**5113-5: The cell update time is in fact the same as the update times for all the nodes. I can't find the exact reference that states this, but it is implied in the RGPS user documentation. If you actually find the node times from the Lagrangian product and compare them to the deformation update times you will find this to be true. This is a bit tricky because the nodes for each cell are not identified, but it can be done. As you indicate, it would make no sense for it to be otherwise.**

Response: Same answer as for the previous question.

Changes: We removed the statements related to asynchronous error.

**5114-13: How are isolated deformation features treated? Is there a minimum kernel size?**

Response: All the selected deformation features are treated the same way. The smoother is applied by averaging the deformation over the cells contained in the kernel only. In the extreme case where the kernel size is 1, the deformation remains then unchanged. There is no minimum kernel size.

Changes: We add this sentence to the paragraph:

“Indeed if a kernel only contains one cell, the smoother does not modify the value of the deformation over that cell.”

**5114-18: Why  $n=3$ ?**

Response: We acknowledge that this choice was not clearly explained in the first version of our paper. From the analysis of the simple test cases,  $n=3$  is chosen as the reference value as it is the only value for which the initial error is at least divided by a factor 3.

Changes:

The choice of the reference value for  $n$  is now explained in the text at the end of section 2.1: “From this analysis, we identify  $n=3$  as an optimal value as it is the only value for which the median error is reduced by at least a factor of 3 in any of the test-cases presented here.

In real cases, to define an optimal value for  $n$  is more difficult as it would depend on the number of intersecting cracks and on the local ratio between divergence and shear. For this study, we chose to use a constant parameter  $n$  and its reference value is fixed at  $n=3$ .

To validate the choice of the method’s parameters (i.e.,  $n$  and the threshold on the total deformation), we present in Sect. 3 another metric based on a multifractal scaling analysis of the deformation fields.” We add in Section 2.2 a reference to Section 2.1: “with the parameter  $n$  equal to 3, which is the reference value defined in Sect 2.1”

**5114-21: For the threshold of 0.02, what is the range of the quality index for different dates in 2006-2007?**

Response: To quantify the range of the quality index, we look at the percentage of pairs of images for the entire winter 2006-2007 for which the quality index is lower than 50% and we found that only 14% of the pairs of images have a quality index lower than 50%.

Changes: We add this information in the text: “To quantify the range of the quality index, we look at the percentage of pairs of images for the entire winter 2006-2007 for which the quality index is lower than 50% and we found that only 14% of the pairs of images have a quality index lower than 50%. To further validate the choice of the model parameters, a consistency check based on a multifractal scaling analysis of the deformation fields is proposed in Sect. 3.”

**5115-25: A shear crack that is not straight may exhibit both opening and closing.**

Response: We agree. A change of orientation of the crack will generate the same problems as the intersections between different cracks. See also our answer to the main comment of reviewer #2.

Changes: We change the word “which” by “where” in the following sentence: “Some features are so polluted by a succession of highly negative and positive values that it is very difficult to identify where cracks are opening, closing or sliding.”

**5116-21: Please give more information about how the scaling was computed. How are the scales determined given that the smoothing introduces a highly variable spatial scale for the individual triangles? Is the area associated with each smoothed triangle retained? How are the strain tensors computed?**

Response: We added more information about the scaling. We do not agree that our smoothing method introduces highly variable spatial scale. The smoothing does not affect the scale at which deformation is defined. This point has been explained in the answer to the second main comment. The area associated with each triangle is the area of the triangle itself even when the deformation has been filtered. As explained in the answer to the remark on line 5111-4, each component of the strain tensor (i.e., the spatial derivatives of the displacement) is averaged.

Changes:

We add this description of the method used for the scaling. The rest of the changes are already described in our answer to the main comment 2 and to the question on line **5111-4**: “Sea ice shear and absolute divergence rates are computed at different spatial scales ranging from 7 to 700 km. For the lowest scale, which is also the scale of the triangular cells, all the cells are taken into account. For the other scales, the coarse graining procedure covers the domain with boxes of different sizes (14, 28, 56, 112, 224, 448 and 896 km). The boxes

actually overlap each other since a distance equal to half the box size separates their respective centers. For each box, we select the cells that have their center in the box. When the sum of the area of those cells is greater than half the box area, the deformation over the box is defined by averaging the spatial derivatives of the displacement weighted by the surface of each cell. The spatial scale for this new estimate of the deformation is the square root of sum of the cells area. The values of deformation obtained for each box size are then reported as a function of the spatial scale on a log-log plot (see Fig. 10 for the absolute divergence rate).”

**5117-10: Please show the results for the RGPS deformation product as well. The unfiltered version of course has very large errors at small scales, as you indicate, so it is of less interest.**

**Response:** It seems that we do not agree with the reviewer on that point. The error (evaluated as the opening/closing error) when using triangles is only about 10% higher than when using quadrangles as in the RGPS deformation dataset (see our answer to the main comment 1). Moreover the RGPS suffers from the distortion of the cells, as the grid is deformed progressively during the season. As explained in the answer to the comment on line 5107-27, these extreme values are difficult to filter and highly influence the multifractal scaling analysis. The presence of these unrealistic deformation values actually necessitates to add extra constraints on the data when performing a scaling analysis. Redefining a new mesh allows us to eliminate most of these erroneous values. Comparing the filtered version to the unfiltered version is then much more interesting because it allows us to clearly identify the impact of the noise on the scaling and the total opening and closing. Moreover, the unfiltered dataset covers exactly the same spatial and temporal domain, and is defined on the same mesh than the filtered dataset. This is not the case for the RGPS deformation dataset, which is even not defined at the same spatial scale (10 km for the RGPS deformation instead of 7 km for our filtered and unfiltered dataset). We then think that it was more interesting to compare the unfiltered and filtered dataset.

However, as asked by the reviewer, we give here the results of the scaling analysis performed on the RGPS deformation dataset. We apply the same constraints on the RGPS deformation data as in Stern (2009), meaning that we add constraints on the size of the cells and we reject the cell whose total deformation is higher than 1% per day. We perform the scaling analysis on the RGPS deformation dataset and we find the same problems as for the unfiltered version of our dataset (i.e., a strong deviation from the power law scaling, see figures 1,2 and 3).

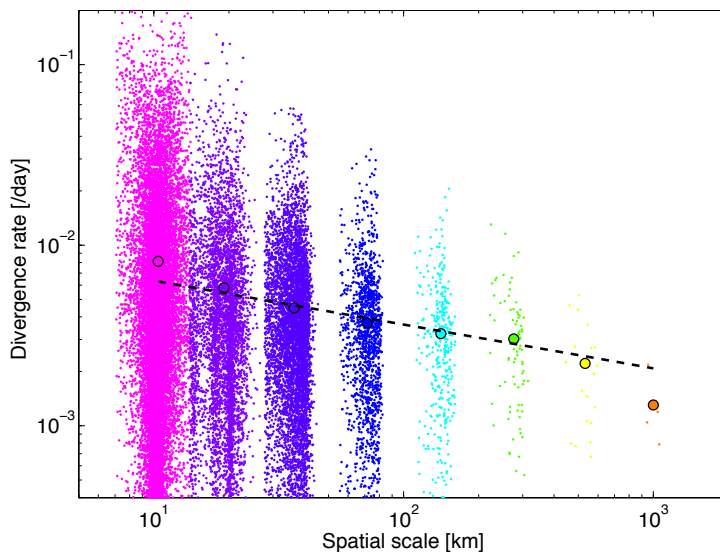


Figure 1: values of divergence (small dots) computed for spatial scales ranging from 10 to 1000 km. The mean values for each scale is shown by a black circle. The dashed line is the best power law fit of the

means. As in the unfiltered deformation obtained on the triangular mesh, a strong deviation from the power-law model is observed for the smallest spatial scales.

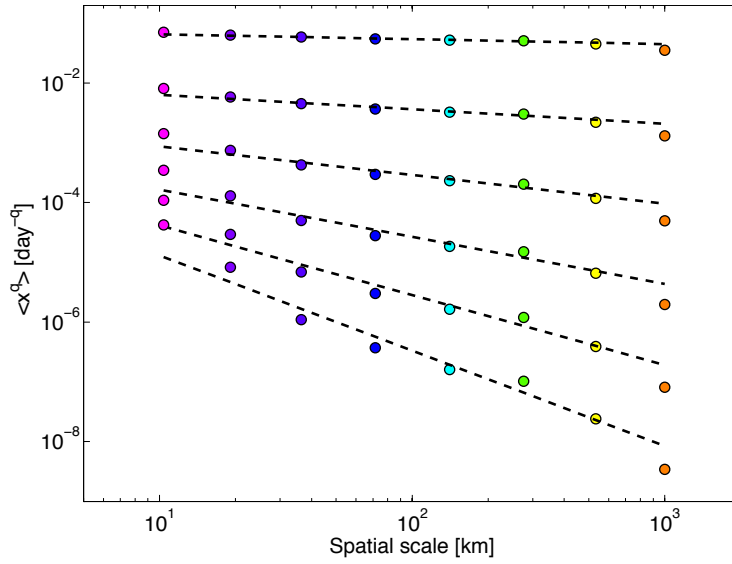


Figure 2: Results of the multifractal analysis applied to the RGPS deformation dataset for the same example as in the paper. As in the unfiltered deformation obtained on the triangular mesh, the strong deviation from the power-law scaling is stronger for the highest moment orders (see the bottom dashed lines).

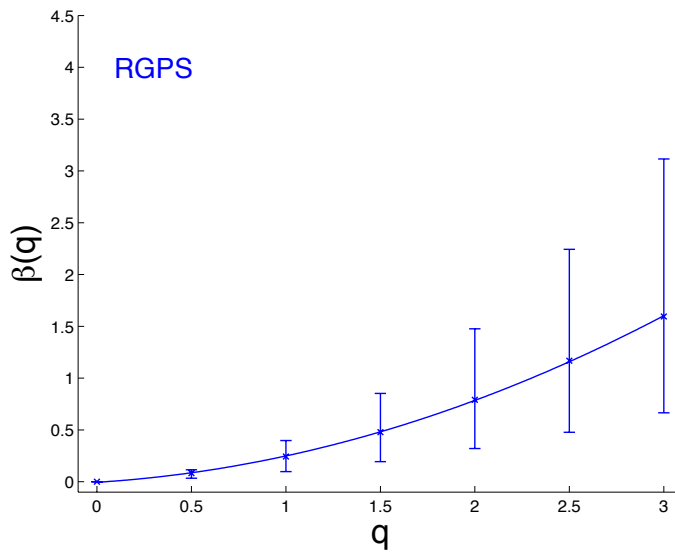


Figure 3: Structure function obtained with the RGPS deformation dataset. The min-max errors are of the same order as the ones of the unfiltered deformation fields presented in the paper.

We think that it is not necessary to include these plots in the paper and that it could bring some confusion among the readers. We think that the comparison of the unfiltered and filtered version of the deformation dataset is cleaner and more robust because we can control all the aspects of the calculation and clearly identify the effect of treating or not the artificial noise. If we restrict the analysis to the comparison with the RGPS deformation dataset, we think it is impossible to correctly assess the effect of the smoother for four main reasons: 1) the domains are not exactly the same, 2) the RGPS deformation suffers from distortion of the cells 3) the initial spatial scales are not the same 4) the RGPS dataset is made using quadrangles instead of triangles, which induces a different error in the unfiltered fields.

Changes: We have added the following statements to explain that we have applied the multifractal analysis to the RGPS deformation dataset and found the same problems as in the unfiltered deformation fields, meaning a strong deviation from the power-law scaling: “We also performed the multifractal scaling analysis on the original RGPS deformation dataset with the same constraints on the data as in Stern (2009) and we found that the departure from the power-law is similar to the one observed for the unfiltered deformation data set.”

**5117-18: What are the min-max errors for some other (n, threshold) pairs? How specific is this optimal solution? And what is it for the RGPS 4-point cell data?**

Response: Figure 4 shows the min-max errors for a threshold parameters ranging from 0 to 0.03 per day. Each curve corresponds to a different moment order (from 3 for the upper curve to 0.5 to the bottom curve). This analysis is done with  $n=3$ . For the threshold parameter, the minimum min-max error for scaling exponent of the third order moment is obtained with 0.02 per day. We acknowledge that the text was not correct, as we said “this combination gives the lowest min--max errors.” but this is not the case for all the moment orders. This mistake is now corrected and we now more clearly indicate the limitations of this analysis and in particular the fact that it is based on a single example. The entire section has been recast as a consistency check rather than a full validation and the statement on the optimality of the value of the parameters have been toned down. See also our answer to main comment 2 of reviewer #2.

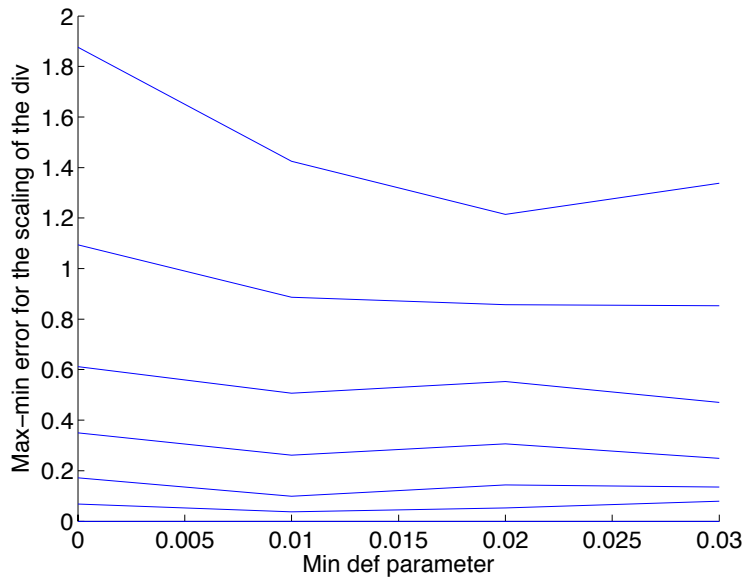


Figure 4

Figure 5 shows the min-max errors for a  $n$  parameters ranging from 0 to 6. Each curve corresponds to a different moment order (from 3 for the upper curve to 0.5 to the bottom curve). This analysis is done with a threshold=0.02 per day. When varying  $n$ , the lowest min-max error for the highest order is obtained with  $n=2$ . The min-max error for order 2.5 is minimum for  $n=3$ . As for the threshold parameter, the value chosen as reference value does not give the minimum min-max errors for all the moment orders. This is now clearly stated in the text.

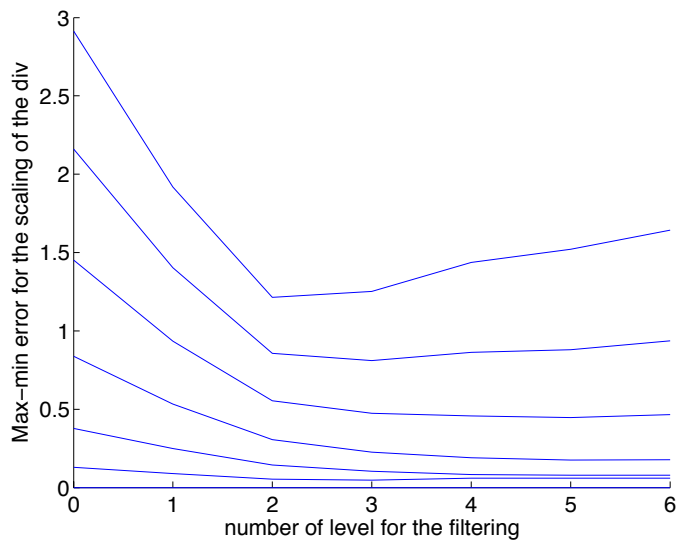


Figure 5

For the RGPS 4-point cell data, the min-max errors are given here above. For the highest order moments (2, 2.5 and 3), the min-max errors with the RGPS deformation dataset are closer to the error obtained with the unfiltered case (i.e., with  $n=0$  on the plot here above) than

with the case filtered with the reference parameters  $n=3$  and  $\text{threshold}=0.02$  per day.

Order moment:	0.5	1	1.5	2	2.5	3
Min-max errors:	0.08	0.30	0.66	1.16	1.77	2.45

Changes:

We adapted accordingly the paragraph on the metric:

“Applied to the composite fields used as example here, we find that using a threshold for the total deformation of 0.02 per day gives the lowest min-max error for the highest order. For the parameter  $n$ , the lowest min-max error for the highest moment order is obtained with  $n=2$ , but  $n=3$  is better for the other moment orders. The application of our metric to this single example tends to indicate that the reference values are well chosen. However, this metric should be applied to a larger number of examples to really identify the best values for the parameters.”

We also add this sentence in the discussion:

“We also performed the multifractal scaling analysis on the original RGPS deformation dataset with the same constraints on the data as in Stern (2009) and we found that the departure from the power-law is similar to the one observed for the unfiltered deformation data set.”

**5118-14: Again, the unfiltered data are of less interest because the 3-point deformations rates are very poorly determined. What are the values for the RGPS data? The whole point of your paper is to improve on the RGPS deformation values, not the unfiltered data set.**

Response: As in the main comment 1 and the comments on 5117-10 and 5107-27, the reviewer argues that the unfiltered deformation field is much worse than the RGPS deformation fields but this is not the case, as explained in our answer to main comment 1 and to the comments on 5117-10 and 5107-27.

The whole point of the paper is to propose a method to reduce the opening/closing error generated by the derivation of the deformation from any motion dataset. The impact of using triangles or quadrangles on the opening/closing error is quite small (10%) compared to the effect of our filtering method, which reduces this error by a factor 8. Moreover the problem of cell distortion present in RGPS data generates ill-defined deformation with unrealistic values that are much higher than in our unfiltered deformation fields. For all these reasons and for those explained in our answer to 5117-10, we decided to not include the scaling analysis of the RGPS deformation dataset in the paper.

We here give the values requested by the reviewer, but we do not include this value in the paper for the reason explained here above. For the snapshot from the RGPS deformation dataset analyzed here, the slope (power law exponent) for  $q=1$  is  $-0.16$  for shear and  $-0.24$  for divergence. The curvature of the structure function is  $0.11$  for shear and  $0.14$  for divergence.

Changes: No changes in the text.

**5120-6: You have not shown how the scaling from the RGPS deformation product differs from that of the new smoothed data set.**

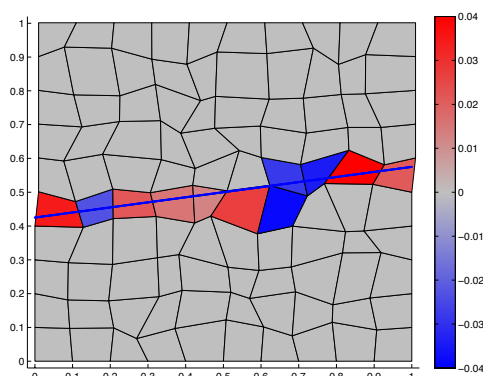
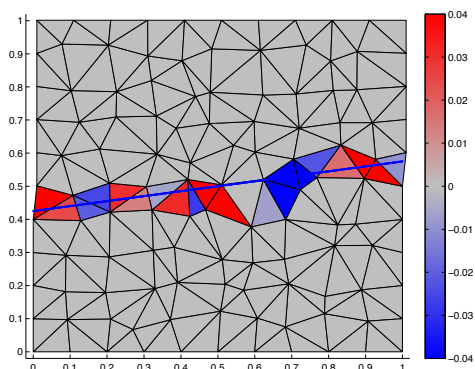
Response: No, we did not because these values may differ for different reasons: the spatial and temporal domain is not exactly the same, the spatial scales are not the same, the criterion to select the data for the scaling analysis are not the same (additional criterion needed for the RGPS deformation to avoid extreme values). See also answer to the comments on 5117-10 and 5118-14.

Changes: We now explain in the text that the RGPS deformation fields present a departure to the power-law scaling similar to our unfiltered fields (see remark on 5117-10).

**Fig. 1: Clearly the classical smoother you use has a much larger spatial scale than the new method. More interesting would be to show what the results would look like for a square grid of nodes, similar to the RGPS cells. Maybe replace the classical smoother, which doesn't make much sense anyway, with a 4-node version. Just define a square grid of nodes and show the deformation for the 4-point cells, for the unfiltered triangles from the same grid, and for the new smoothed version.**

Response: We think showing results with the classical smoother makes sense, as it illustrates the classical approach of just taking more points to compute the deformation. The example in Figure 1 has 29 points on the circumference of the region and then corresponds to compute the deformation with a large cell defined by these 29 points. Computing the deformation with 4-points is just another application of the same idea and it has the same drawback: it changes the spatial scale at which the deformation is defined and does not significantly reduce the noise.

We prefer to keep our example with the classical smoother as it clearly shows that our approach is different than the classical approach of just defining larger cells. It also allows us to introduce the smoothing method. We do not think that comparing the results on triangular and quadrangular meshes, as in the following figures, would be useful. As we already explained, the total opening/closing error obtained with the triangles is just 10% higher than with quadrangles.



Changes:

We now specifically explain how our filtering method does not induce a change in the spatial scale at which deformation is defined. See also our answer to main comment 2

**Fig 3: What is normalized resolution?**

Response: It is the mean distance between the points used for the simple test cases. It is called normalized resolution as it is defined for a normalized area equal to 1 and should not be confounded with the resolution of the meshes build for real cases.

Changes: We have now added this sentence to the first paragraph of section 2.1: “d is hereafter called the normalized resolution.” We do not change the caption of this figure.

**Fig.6: Please add the black triangles here too so we can see which are smoothed.**

Response: To keep the same visual aspect as the for unfiltered divergence fields we prefer not to add black triangles on figure 6.

Changes: We add in the caption of figure 6:

“The triangles that have been treated by the smoother are those in black in Fig. 5. For the other triangles, the value of the deformation remains the same as in Fig. 4”.

**Figs 10-12: What are the scaling relationships for the RGPS deformation data? The unfiltered data is not very interesting, since you have added a lot of noise by using just three points at the smallest scale. The more interesting question is how the RGPS data compares.**

Response: Same answer as for the question 5117-10.

Changes: No change has been made for these figures.

## Response to reviewer #2

We first would like to sincerely thank the reviewer for his throughout review and his numerous useful comments that, we believe, contribute to significantly improve our manuscript. Each answer/comment of the reviewer below is followed by a "response" and when applicable by a more specific description of the "change(s)" we made to the manuscript.

### General comments

**My main comment is: how do the authors know that the observed openings and closings along a lead are actually "noise" and not "signal"? In the real world, a lead is not necessarily a perfectly straight line with smooth sides. Little "jogs" along the main direction of the lead will give rise to openings and closings even under pure shear deformation. These little jogs cannot necessarily be resolved by the 10-km spacing of the grid points.**

**Consider, for example, the situation in Figure 1(a). Suppose the crack, depicted as a thick black line, actually has a small "jog" in it – a section of length  $W = 0.01$  perpendicular to the main direction of the crack. (Note that the spacing of the points is about  $10^4 W$ ). The points above the crack have a relative displacement parallel to the crack of  $U = 0.01$ . This gives rise to an unmeasured opening (or closing) of area  $U^*W$  within the triangle where the jog occurs. Since there are about 200 triangles in the figure, each one has an area of about 0.005. Therefore the relative area change (divergence) due to the jog would be  $U^*W/0.005 = 0.02$ , which is roughly the magnitude of many of the red triangles along the crack. The point is: small unresolved jogs along the length of a crack will in fact give rise to small amounts of opening and closing under pure sliding deformation. In an idealized situation where the crack is assumed to be a straight line, the openings and closings as in Figure 1(a) are certainly noise. But in a real-world situation, it is not necessarily unphysical to have openings and closings along a crack. The only way to really figure out what's going on is to go back to the original SAR imagery and track more points along the boundaries of the cells, in order to get better representations of the true material boundaries of the ice. But I am not suggesting that the authors need to do this – it would be far too much work.**

**Consider another case where a horizontal crack with a small vertical jog passes through the middle of a square cell, and the ice slides along the direction of the crack. As above, this gives rise to an actual opening (or closing) within the cell, but the shape of the cell changes from a square to a rhombus with no change in area. In this case, the unfiltered ice motion field produces an UNDERestimate of the true opening. The point is: the unfiltered fields can give rise to UNDERestimates of the true divergence as well as OVERestimates.**

**What the authors have actually done is to show that their filtered fields lead to better agreement with power-law scaling behavior than the unfiltered fields. This is not exactly "validation", it's really a consistency check with the assumption that the deformation should have power-law scaling. Real validation would involve finer-scale ice tracking (as noted above) or an independent data set. However, the consistency check does lend credibility to the authors' method of filtering the data.**

**In summary, my main comments are: (1) the "artificial noise" may actually contain some valid "signal" in real-world situations, and (2) the "validation" is really a consistency check. The authors need not re-do any of their analysis, but I think they should acknowledge these points.**

#### Response to main comment (1):

Sea ice deformation is defined at a given scale. The deformation computed at the scale of the data (10 km) is therefore not the same as the one computed at lower scales. The aim of this paper is to increase the accuracy of the deformation fields computed at the resolution of the

data (e.g., at 10 km when using the SAR-derived ice drift like in the RGPS data). We think that the term “true divergence” is ambiguous, as it does not refer to a specific spatial scale. We think that the remark of reviewer could be reformulated as: “What valid information can we derive from the deformation at 10 km on the deformation at smaller scales, for example at the field scale, i.e.  $\sim 1\text{m}$ ?”. The answer would be that it is possible to extrapolate the distribution of the deformation at smaller scales by using the information retrieved from the multifractal scaling analysis. It has been done in Marsan et al. 2004 to determine the distribution of the total deformation at a spatial scale of 1 m. We have not done this extrapolation in the present paper but it would bring valuable information on the opening/closing (in other words, the absolute divergence) experienced by sea ice at smaller scales. It should be noted that we provide a more accurate estimate of the power-law exponents of the spatial scaling as the corresponding uncertainty associated to the power law fit significantly decreases after removing the noise following the presented method. As a result, the extrapolation at smaller scales would be more accurate. However, as we have not yet investigated this idea, we will not include any statement on the extrapolation to smaller scales in the paper.

Once this ambiguity about the definition of the deformation is cleared, we can answer to the specific remarks of the reviewer:

In the “real-world” the “little jogs” described by the reviewer are observed on a wide range of scales (see the description of the secondary cracks in Schulson (2004)). The presence of these features at all scales is partly responsible for the spatial scaling of the deformation. However, as explained by the reviewer, the resolution of the data limits the representation of these features. A dataset having a resolution of 10 km is only able to “see” “little jogs” longer than 10 km. In consequence, the deformation values, but also integrated quantities, for example the total opening/closing, will not be the same when computed at a resolution of 10km or at higher resolution.

The reviewer suggests using data at higher resolution, but, as shown in section 2.1 with the idealized test cases, the opening/closing error generated by the artificial noise does not depend on the resolution. In the idealized test cases, unfiltered deformation fields at higher resolution have the same error as unfiltered deformation fields at lower resolution. To apply the suggestion of using higher resolution, one should therefore also filter the deformation computed from high-resolution data. The suggestion of using independent dataset has been added to the conclusion. We are already working on that topic.

Concerning the example with a “little jog” added to the single crack experiment, we agree on the figures computed by the reviewer. As explained by the reviewer, the presence of a “little jog” “... gives rise to an unmeasured opening (or closing) ... within the triangle where the jog occurs”. The unmeasured opening or closing is then of the same order of magnitude as the artificial opening/closing in the unfiltered field. Therefore, in the worst case, this unmeasured opening or closing may double the local error in one cell. However, in other cases, it could also reduce the local error when the artificial and unresolved opening/closing has the same magnitude but opposite sign. On average, it will then likely have no impact on the total opening/closing error obtained from a large set of experiments.

Concerning the second example with a unique triangle in which a “little jog”, we also agree with the description made by the reviewer but we think that his conclusion: “In this case, the unfiltered ice motion field produces an UNDERestimate of the true opening.” is ambiguous. First of all, this sentence is only true when looking at one specific triangle. When looking at the total opening/closing over the square domain, the local underestimation of the opening is much lower (one order of magnitude) than the total overestimation of the total opening/closing generated by the artificial noise. Secondly, this analysis is only true for a cell having a specific orientation relative to the crack (a triangle or a square with an edge parallel to the crack). When looking at a large number of experiments (with random orientation of the cracks and of the direction of the little jog), the opening/closing in the triangle with the “little jog” will equivalently be OVER and UNDERestimated. The median error will likely not be affected by the presence of a little jog. **The conclusion of the reviewer: “the unfiltered fields can give rise to UNDERestimates of the true divergence as well as OVERestimates” only**

**reflects the presence of noise in the unfiltered deformation field.** It does not apply to the constant overestimation of the opening and closing rate caused by the artificial noise. We think that our definition of the error is clear enough, and does not necessitate any change. We always compute the error over the analyzed domain and not the local error that is actually equivalent to noise.

Concerning the suggestion of the reviewer, we cannot agree to say that: “artificial noise” may actually contain some valid “signal” in real-world situations. In particular, we think that the “artificial noise” perturbs the “signal” so strongly that it actually makes it impossible to retrieve valid information about the deformation experienced by the sea ice. We showed that the “artificial noise” generates an overestimation of the deformation at 10 km and an overestimation of the scaling exponents. This deviation from the power-law scaling when the spatial scale reaches the data resolution clearly suggests that this noise is artificial and not linked to real properties of sea ice deformation.

Changes for main comment (1):

We add to the conclusion:

“A complete validation using independent datasets should also be done.”

Response to main comment (2):

We agree.

Changes for main comment (2):

As suggested by the reviewer, we renamed the section “Validation” into “Consistency check” .

### **Specific Comments**

**Page 5106 line 17. Cross correlation and feature tracking in SAR images go back decades to the work of Fily and Rothrock (JGR-Oceans 1990) and Kwok et al (IEEE J Ocean Engr 1990).**

Response: Yes, we agree.

Changes: We have added those references.

**Page 5106 line 20. A better reference for RGPS is: Kwok, R., The RADARSAT Geophysical Processor System. in Analysis of SAR data of the Polar Oceans: Recent Advances, Tsatsoulis, C. and R. Kwok, Eds.: 235-257, Springer Verlag, 1998.**

Response: Yes, we agree.

Changes: We now use this reference.

**Page 5106 lines 20-21. "Central Arctic" should be changed to "Western Arctic". Look at the coverage map in Figure 7.**

Response: Yes, we agree.

Changes: It has been corrected.

**Page 5108, The method involves a triangulation of a set of tracked points. The deformation is calculated for each triangle. Note that a triangle is the least accurate shape one can possibly use for calculating sea ice deformation. The problem is this: in estimating the deformation of a region using a discrete set of boundary points, the implicit assumption is that the points adequately resolve the material boundary of the region. In other words, as the shape evolves over time, there should not be a flux of ice into or out of the region. But the sides of a triangle will almost certainly not be material boundaries unless all three vertexes are on the same rigid piece of ice (in which case the deformation is zero). The more points that are used to define the boundary, the more accurate the estimate of the deformation becomes. Thorndike (Kinematics of Sea Ice, Chapter 7 in The Geophysics of Sea Ice, NATO ASI Series, vol 146, 1986) found that the ratio of estimation error variance to signal variance is about**

0.7 when using 3 points to estimate divergence (see Fig 23b and the discussion at the top of page 536). This ratio drops significantly for 4 points and 5 points. As the authors point out later, triangles give the best spatial resolution, but it should be noted that they also give the worst accuracy. However, the filtering scheme used by the authors effectively increases the number of boundary points that define the material element containing a crack, thereby improving the accuracy of the deformation estimate in that element. When the spatial ice motion derivatives within two or more adjacent cells (triangles) are averaged together, the contributions from the internal cell boundaries cancel one another, leaving only the contributions from the external cell boundaries. This effectively creates one large cell in which the derivatives are the same as if they had been calculated by a contour integral around the outer boundary, as in equations 1-4. Thus the cell-by-cell averaging can also be viewed as a way to combine the cells into one larger cell for which the material boundary is defined by many points. I think this is worth noting.

Response :

We agree with the reviewer that the problem partly concerns the identification of individual objects or of the boundaries between individual objects. As stated in the conclusion, the inclusion in tracking algorithms of strategies to detect discontinuities (as in Thomas (2008)) could solve this problem by providing much better definition of these boundaries.

We appreciate that reviewer fully understand the spirit of our method which is actually a combination of a detection method and a smoothing method.

Concerning the error introduced by using triangles, please read our answer to General comment 1 of reviewer #1.

Changes: No change linked to this remark.

**Page 5110 and following. The letter "n" is used to mean 4 different things: - The number of vertexes of a grid cell. See page 5110 line 3 ( $n=3$ ) - A subscript on epsilon to indicate divergence. See page 5110 equation 7. - A subscript on u to indicate the velocity component normal to the crack. See page 5110 line 10. - The number of triangle edges that are crossed in order to construct the smoothing kernel. See page 5110 line 25 ( $n=7$ ). It is possible that the reader may become confused about the multiple uses of "n".**

Response: Yes, we agree.

Changes: The number of vertexes is now indicated by letter "m". The subscripts for epsilon are now "div" and "shear". "n" is kept for the subscript on the normal displacement. Italic "n" is kept for the number of triangles that can be crossed to create the smoothing kernel.

**Page 5111, line 12 and following. The 2 parameters in the filtering method are the deformation threshold and the size of the kernel. "the threshold value is chosen to be small enough to select all the deforming cells" (lines 14-15). That's all we're told (here) about how to select the threshold. Later, at the top of page 5114, the authors explain more about the choice of threshold. It would be helpful to say on page 5111 that more details about choosing the threshold are presented later.**

Response: Yes, we agree.

Changes: We add this sentence: "For application to real data, the choice of this parameter is critical and is detailed in Section 2.2."

**Page 5113 lines 18-19. Yes, using triangles instead of quadrilaterals increases the number of deformation estimates and increases the resolution, but it decreases the accuracy of the estimates. See the previous comments about "Method".**

Response: We agree that the uncertainty (here defined as the opening/closing error) is slightly higher with triangles than with quadrangles. It is now explicitly shown in Section 2.1.

However, using triangles has another great advantage. Triangulations can be applied to any set of points, which is not the case for quadrangulations.

Changes: We now have a full paragraph to justify the choice of using triangular meshes: "Using triangles instead of quadrangles roughly doubles the number of deformation estimates, and increases the resolution of the deformation product up to 7 km. Another advantage is that triangulations can be made on any set of points (if they are not all aligned), which is not the case with quadrangulation (Bremner, 2001). If the tracked points are given on a regular grid, quadrangulation could be easily performed and could be preferred to start with a reduced uncertainty on the initial unfiltered fields. However for most of the available datasets (for example GlobICE and EGPS), the data are not given on a grid but as a list of points. The method presented here based on triangles is then very flexible and can be applied to many different sources of data. In the next section, the unfiltered and filtered deformation fields obtained on triangular meshes are compared to the RGPS deformation fields. The smoothing procedure is not applied to the RGPS deformation fields because it requires to know the neighbors of each cell and this information is not present in the RGPS Lagrangian deformation dataset."

**Page 5113 line 29. I don't understand what this means: "while keeping an important weight for the shear deformation"**

Response: We agree that the end of the sentence was not clear.

Changes: As this part of the sentence was also not necessary, we removed it.

**Page 5114 lines 9-16. I don't understand the quality index – neither how it's defined nor how it's used.**

Response: We now specifically introduce a notation for the size of the kernel and we explain with the test-cases how we determine that the size of the kernel  $IK_{sl}$  could be as low as  $n+1$  for single cracks when the center of the kernel is at the boundary of the mesh and as high as  $4n+1$  for two intersecting cracks. This is now explained in the text and we also add several sentences to explain how we use this quality index to determine the reference value for the threshold parameter.

Changes: Here are the sentences added to the text:  
"Based on this quality index, the threshold values 0.01 and 0.02 per days are the best. The value of 0.02 per day is chosen as the reference value for the deformation threshold. To quantify the range of the quality index obtained with this reference value, we look at the percentage of pairs of images for the entire winter 2006-2007 for which the quality index is lower than 50% and we found that only 14% of the pairs of images have a quality index lower than 50%. To further validate the choice of the model parameters, a consistency check based on a multi-fractal scaling analysis of the deformation fields is proposed in Sect. 3."

**Page 5116 lines 8-9. The authors state that the scaling analysis is very sensitive to the presence of noise in the analyzed field. But the scaling analysis is done with the MEAN deformation, which is the result of averaging over many values, which greatly reduces the noise. See line 23: the mean value  $\langle \epsilon_{L} \rangle$  is used. See also Figure 10: the huge cloud of points at each spatial scale is averaged to produce a single mean value (the black circle), which surely is not very sensitive to noise in the analyzed field, even at the 200-km scale, where the sample size is still reasonably large.**

Response: We agree that our statement was too general to be always true. We change it into a more specific description of how the noise in the deformation field modifies the distributions of absolute divergence and shear, and how it impacts the spatial scaling. We also specifically indicate that it is the absolute divergence on which the scaling analysis is performed. This point was maybe not stressed enough and this could explain the question raised by the

reviewer.

Changes: “The spurious noise in the deformation fields corresponds to high values of deformation and is potentially present for any active linear kinematic features. This noise may then impact the distributions of absolute divergence and shear and modify their mean (1st-order moment) but even more their standard deviation (2nd-order moment) and skewness (3rd-order moment). Moreover this noise is the highest at the resolution of the data but rapidly decreases for larger spatial scales. We then expect that the presence of noise in the deformation fields will have a strong impact on the result of the scaling analysis, especially for the smallest scales and the highest-order moments of the distribution.”

**Page 5117 lines 3-4. "The artificial noise particularly induces a strong departure from the power-law model at the smallest scales (see Fig. 10)" I don't see the strong departure. In Fig 10 (left panel, unfiltered), at the smallest scales, it looks to me like the dotted line (power law model) is quite close to the black circles (mean deformation).**

Response: For the filtered data all the circles from 7 to 200 km are well aligned with the dashed line and this is clearly not the case for the unfiltered data. We agree that some of the black circles for the unfiltered data are close to the dotted line but not all of them, meaning that the unfiltered data do not follow the power-law model.

Changes:

We now more precisely describe the results of the scaling analysis for the filtered and unfiltered data. The following text has been added and is followed by the description of how the scaling of the unfiltered data deviates from the power-law scaling for the scales smaller than 50 km.

“The filtered shear and absolute divergence closely follows the power-law model for the spatial scaling as their first order moments are well aligned with the power-law fit for the spatial scales ranging from 7 to 200 km (see right panel of Fig. 10 for the absolute divergence). This is not the case for the unfiltered deformation fields (see left panel of Fig.10) and we explain this strong departure from the power-law model by the presence of artificial noise.”

**Page 5117 lines 11-18. My understanding is that the authors are trying to find the set of method parameters that gives the best linear relationship between deformation and spatial scale (in log-log space). This could be done using standard least-squares fits, with standard measures of the goodness-of-fit such as the squared correlation  $R^2$ , for each set of method parameters. Instead, the authors invent their own procedure for finding the best set of parameters, by calculating slopes for each successive pair of spatial scales and then using  $\max(\text{slope}) - \min(\text{slope})$  as the "error" to be minimized. Why not use a standard method like least squares? The authors' method would appear to be very sensitive to outliers. Can they give assurances that their method is "reasonable", or cite a reference for it?**

Response: The choice of the method (i.e., the definition of the error by the min-max error) is motivated by the fact that we want to quantify the deviation from the power-law scaling. By definition, if a scaling holds for a given range of scales, it should be respected for any pair of scales within this range. We perfectly understand that our measure of the error is very sensitive to “outliers” and this is precisely what we want. We want to be sure that when we define a power-law exponent for the scaling over a given range of spatial scales, this exponent will be the same (or very close) for any pairs of spatial scale within this range. This information will not be given by squared correlation. It should be noted that the term “outliers” is here applied to the mean values of the shear or absolute divergence (black circles). These mean values are obtained as the average of a very large number of points, meaning that any small deviation from the power-law scaling cannot be caused by only a few outliers in the deformation datasets but by the presence of a large number of artificially high values of deformation.

**Changes:** We add a new paragraph in this section to present the definition of our error bars: "By definition, if a scaling holds for a given range of scales, it should be respected for any pair of scales within this range. To evaluate the deviation from the power law scaling, we compute the power-law exponents for each pair of successive spatial scales (i.e. from 7 to 14 km, from 14 to 25 km, and so on) and we take the minimum and maximum values of these exponents. Those values as well as the exponents previously obtained with the whole range from 7 to 20 km are reported as a function of the moment order  $q$  in Fig. 12. The relationship between the power-law exponents and the moment order  $q$  is called the structure function  $\beta(q)$  and is defined by  $\langle \dot{\epsilon}_L^q \rangle \propto L^{-\beta(q)}$ . The minimum and maximum exponents define the bars around  $\beta(q)$ ."

See also the response to the question 5117-18 of reviewer #1 on the choice of the model parameters.

### Technical Corrections

**Title of paper. The word "dataset" should be plural: datasets. Also, the editors of the journal need to decide whether "datasets" is in fact one word or whether it should be "data sets". I use two words, but the journal might have a different convention.**

**Response:** We agree.

**Changes:** We now use the plural in the title. We leave the editor decide if we should use the term "data set" instead of "dataset".

**Page 5106 line 26. Kwok and Stern 1995 is actually Kwok, Rothrock, Cunningham, and Stern 1995.**

**Response:** Thank you.

**Changes:** Reference corrected.

**Page 5112 line 21. "position" should be plural: positions.**

**Response:** Thank you.

**Changes:** It has been corrected.

**Page 5112 line 24. Put the word "negative" before "y axis": the negative y axis is aligned with the 45W meridian.**

**Response:** Thank you.

**Changes:** It has been corrected.

**Page 5113 line2. "first ... secondly" should probably be "first ... second"**

**Response:** Thank you.

**Changes:** This sentence has been modified and does not contains these terms anymore.

**Page 5115 lines 8 and 9. Maybe the word "large" should be "long"?**

**Response:** Thank you.

**Changes:** It has been corrected.

**Page 5118 line 8. The scaling exponents are "systematically higher". The word "higher" is ambiguous because the quantities in question are negative. "higher" could mean "higher in magnitude" (more negative) or "higher in value" (less negative). I'd suggest either "larger in magnitude" or "more negative".**

**Response:** Thank you.

**Changes:** It has been corrected, we use now "larger in magnitude".

**Page 5119 line 7. "drops" should be "drop"**

**Response:** Thank you.

**Changes:** It has been corrected.

**Page 5119 line 10. "cumulated" should be "cumulative"**

Response: Thank you.

Changes: It has been corrected.

**Page 5120 line 13. "buoys trajectories" should be "buoy trajectories"**

Response: Thank you.

Changes: It has been corrected.

**Figure 10. What do the colors mean? They should be explained in the caption.**

Response: Each color corresponds to a different box size used for the coarse graining procedure.

Changes: It is now indicates in the caption.

Manuscript prepared for The Cryosphere Discuss.  
with version 2014/09/16 7.15 Copernicus papers of the L<sup>A</sup>T<sub>E</sub>X class copernicus.cls.  
Date: 2 February 2015

# On producing sea ice deformation **dataset** datasets from SAR-derived sea ice motion

**S. Bouillon<sup>1,2</sup> and P. Rampal<sup>1,2</sup>**

<sup>1</sup>Nansen Environmental and Remote Sensing Center, Bergen, Norway

<sup>2</sup>Bjerknes Centre for Climate Research, Bergen, Norway

Correspondence to: S. Bouillon (sylvain.bouillon@nersc.no)

## Abstract

We propose a method to ~~compute nearly noise-free~~ reduce the error generated when computing sea ice deformation fields from SAR-derived ~~motion and present the results of its application to RGPS sea ice trajectories~~ sea ice motion. The method is based on two steps. The first step consists of using a triangulation of the positions taken from the sea ice trajectories to define a mesh on which a first estimate of sea ice deformation is computed. The second step consists of applying a specific smoother to the deformation field to reduce the artificial noise that arises along discontinuities in the sea ice motion field. This method is here applied to RGPS sea ice trajectories having a temporal and spatial resolution of about 3 days and 10 km, respectively. From the comparison between unfiltered and filtered fields, we estimate that the artificial noise causes an overestimation of about 60 % of opening and closing. The artificial noise also has a strong impact on the statistical distribution of the deformation and on the scaling exponents estimated with ~~multi-fractal analysis~~ multifractal analysis. We also show that a similar noise is present in the deformation fields provided in the widely used RGPS dataset. These findings may have serious implications for previous studies as the constant overestimation of the opening and closing could lead to a large overestimation of freezing in leads, salt rejection and sea ice ridging.

## 1 Introduction

Sea ice motion can be retrieved from satellite SAR images using cross correlation techniques and feature tracking algorithms (~~Hollands and Dierking, 2011~~) (Kwok et al., 1990; Fily et al., 1990; Hollands and Dierking, 2011). Sea ice deformation is then estimated by computing the spatial derivatives of the sea ice motion. The most popular dataset providing both sea ice motion and deformation is the RADARSAT Geophysical Processor System (RGPS) dataset (Kwok, 1998). It covers the ~~Central~~ Western Arctic for the period 1996–2008 at temporal and spatial resolution of about 3 days and 10 km, respectively.

As deformation determines sea ice opening (i.e. positive divergence) and closing (i.e. negative divergence), it may be used to estimate important global quantities, such as the ice production in leads, with some assumptions on sea ice growth and redistribution (Kwok et al., 1995). Using the RGPS dataset, Kwok (2006) estimated that deformation-related ice production is about 25–40 % of the winter ice production in both the perennial and seasonal ice zone. Kwok et al. (2008) also showed that the deformation-related ice production derived from the RGPS dataset is up to two times higher than the one estimated by numerical models, implying a potential underestimate of the associated sea ice–ocean feedbacks.

In addition to essential information about sea ice opening and closing, the analysis of sea ice motion and deformation also gives a particular insight to the underlying physics controlling the sea ice dynamics and provides precious information with which to validate sea ice models. Marsan et al. (2004) described how the statistics of sea ice deformation vary as a function of spatial scale, while Rampal et al. (2008) generalized these scaling properties to both the spatial and temporal domains. Stern and Lindsay (2009) and Herman and Glowacki (2012) documented the seasonal and inter-annual variability of the spatial scaling exponents. Girard et al. (2009, 2011) showed that classical sea ice models do not capture these statistical properties.

The estimation of these global quantities (e.g. total opening/closing) and statistical properties (e.g. spatial scaling exponents) may be impacted by errors in sea ice deformation data. Uncertainty on deformation is usually seen as a consequence of motion tracking errors that depend on the algorithm and parameters used. Lindsay and Stern (2003) estimated the standard deviation of the error in area change to be about  $1.4 \text{ km}^2$  for a 10 by 10 km cell when the tracking error (i.e. tie point) is about 100 m. This error estimate is equivalent to the level of significance of 0.005 per day for 3 day intervals estimated by Kwok and Cunningham (2002), and used to determine the error on ice production as being less than 1 % of the total.

However, two other sources of error can be identified. Both are linked to the definition of the boundary of the cell (usually quadrangle) over which deformation is computed. Lindsay

and Stern (2003) showed that unrealistic deformation is often obtained when this boundary is too irregular. Also, spurious openings and closings (that we will refer to as artificial noise hereafter) are caused by unfavorable orientation of the cell boundary relative to the discontinuities in the sea ice motion field, also called dynamic discontinuities, slip lines or linear kinematic features. Lindsay and Stern (2003) evaluated the standard deviation of the error in area change due to the boundary definition to be about  $3.2 \text{ km}^2$  for a 10 by 10 km cell, which is more than twice the error from tracking mentioned above. Kwok (2006) stated that this artificial noise would lead to an overestimation of the ice volume production, although no precise number was given. Lindsay et al. (2003) proposed to reduce this error by combining cells together, but this solution reduces the benefits of having high resolution data and reduces the spatial range over which one could perform scaling analysis.

This paper proposes a method to avoid unrealistic values and to significantly reduce the noise obtained when computing sea ice deformation from SAR-derived motion and presents an example of its application to sea ice trajectories coming from the RGPS dataset. The complete method is described in Sect. 2. In Sect. 3, we discuss the quality of the obtained deformation fields and we analyze the impacts of removing the artificial noise on the estimated global opening/closing and on the spatial scaling of the deformation. Section 4 concludes the paper with a discussion on potential improvements of the method and on implications of our findings for the existing literature.

## 2 Method

The method we developed is based on two steps. The first step consists of defining a mesh by doing a triangulation of a set of tracked points. For each individual triangular cell, the deformation is calculated using the motion of its three nodes estimated from the tracking procedure. The second step consists of applying a specific smoother to the obtained deformation fields to reduce the artificial noise.

## 2.1 Application to simple test cases

In order to present the method, we first define a simple setup on a square domain having a normalized area equal to 1. In this domain, tracked points are distributed uniformly with a mean distance  $d$  between them (see for example Fig. 1 with  $d = 0.1$ ).  $d$  is hereafter called the normalized resolution.

In the first test case, a single crack is defined (black line on Fig. 1). This crack passes by the center of the domain and makes an angle  $\theta$  with the horizontal  $x$  axis. We want to simulate a discontinuous displacement field that is induced by the presence of that crack. To do so, we keep the points located below the crack (lower part of the domain in Fig. 1) as fixed, and we require the points above the crack (upper part of the domain in Fig. 1) to move with the same displacement. The two components of the imposed displacement,  $u_p$  and  $u_n$ , correspond to the displacement parallel and normal to the crack, respectively.

The first step of the method is to perform a Delaunay triangulation of these points to generate a mesh on which deformation is computed. The spatial derivatives of the displacement are obtained by calculating the following contour integrals as in Kwok et al. (2008) around the boundary of each triangle:

$$u_x = \frac{1}{A} \oint u dy \quad (1)$$

$$u_y = -\frac{1}{A} \oint u dx \quad (2)$$

$$v_x = \frac{1}{A} \oint v dy \quad (3)$$

$$v_y = -\frac{1}{A} \oint v dx, \quad (4)$$

where  $A$  is the **encompassed cell** area. For example,  $u_x$  is approximated by:

$$u_x = \frac{1}{A} \sum_{i=1}^{nm} \frac{1}{2} (u_{i+1} + u_i)(y_{i+1} - y_i), \quad (5)$$

where  $n=3$  and subscript  $n+1=1$ ,  $m=3$  and subscript  $m+1=1$ . The shear  $\epsilon_s$  and divergence  $\epsilon_{n\text{div}}$  deformations are computed as:

$$\epsilon_{s\text{shear}} = \sqrt{(u_x - v_y)^2 + (u_y + v_x)^2}, \quad (6)$$

$$\epsilon_{n\text{div}} = u_x + v_y. \quad (7)$$

In the case of a slip line,  $u_n$  is set to zero. No opening or closing should occur and shear should have the same value along the crack. Figure 1a and b show the divergence and shear computed for such a case, with  $u_p = 0.01$  and  $u_n = 0$ . The divergence field exhibits spurious positive (opening) and negative (closing) values along the slip line. The shear field also exhibits some noise, but that is hardly visible on the figure.

This artificial noise generates an overestimation of the total opening (and closing). Repeating the slip line ~~experience experiment~~ 100 times, with  $\theta$  varying from  $-\arctan(0.2)$  to  $+\arctan(0.2)$  and with different meshes, we find that the ~~rms root mean square (rms)~~ error per unit crack is about 20 % of the sliding distance  $u_p$  for both the opening and closing. In other words, with a 100 km long crack and a sliding distance of 1 km, the artificial opening (and closing) would be about 20 km<sup>2</sup>. It is particularly interesting to note that this error does not depend on the normalized resolution  $d$  (we tested with  $d$  equal to 0.1, 0.01 and 0.001).

When repeating the same test case with quadrangles instead of triangles, we found a rms error of about 18 % of the sliding distance  $u_p$ . For comparison, Lindsay and Stern (2003) found an error per unit crack of about 15 % of the sliding distance, for a similar test case on a mesh made of square cells. ~~It is particularly interesting to note that this error does not depend on the normalized resolution  $d$  (we tested with  $d$  equal to 0.1, 0.01 and 0.001)~~ This analysis shows that using triangles only generates an increase of about 10 % of the opening (and closing) error compared to using quadrangles. This increase of the

error is minor compared to the advantages of using triangles. Triangulation methods are more flexible. It roughly doubles the number of deformation estimates and it increases the resolution at which deformation is defined. For the rest of this paper, we then only present results on triangular meshes but the method could also be applied to other type of meshes.

In order to remove the artificial noise in the deformation fields one could apply a ~~typical smoother~~. For example, we can define a kernel around each individual cell as the set smoother over all the cells of the mesh. We here denote  $C$  the list of all the cells and for each cell  $c \in C$ , we define the kernel  $K_c \subset C$  as the subset of cells that can be reached by crossing a maximum of  $n$  edges (see. An example of kernel with  $n = 7$  is shown in Fig. 1c and d for an example with  $n = 7$ ). The size of the kernel is noted  $|K_c|$ . For the example shown in Fig. 1c and d,  $|K_c|$  is equal to 87. The components of the filtered deformation are then defined by averaging local derivatives over the selected cells as an area-weighted average over the cells of the kernel. For example, the filtered value for  $u_x$  on the cell  $c$  is defined as

$$\tilde{u}_x^c = \frac{\sum_{k \in K_c} A^k u_x^k}{\sum_{k \in K_c} A^k}. \quad (8)$$

This method reduces part of the artificial noise but is not appropriate since it ruins the localization of the shear and adds unreal deformation to non-deforming cells. It also modifies the spatial scale at which the deformation is defined, resulting in a modification of the value of the shear along the crack. With the single crack case, the area-weighted average of the shear for the cells cut by the crack is found to be inversely proportional to  $n$ .

We propose a better method based on the fact that the deformation is by nature constant along a linear kinematic feature. Averaging motion derivatives along these features could then filter out the noise without spoiling the information on the real deformation. Contrary to the smoother presented here above, the scale at which the deformation is defined remains constant with the second method. In other words, the mean value of the shear along the crack obtained with the second method does not vary as a function of  $n$ . We also verified that in the case of a regular mesh and a single crack aligned with the

x-axis, the area-weighted average of the shear along the crack is strictly constant whatever the value of  $n$ .

To detect the cells that are involved in the mapping of each linear kinematic feature, we define a threshold for total deformation ( $\sqrt{\epsilon_n^2 + \epsilon_s^2} \sqrt{\epsilon_{div}^2 + \epsilon_{shear}^2}$ ). Only the cells whose total deformation is above the threshold are ~~taken into account~~ selected to build the smoothing kernels (see Fig. 1e and f for an example with  $n = 7$ ). ~~Thanks to this preselection of cells, our method reduces the noise while preserving the~~ No filtering is applied on the cells where deformation is below the threshold. We denote  $S$  the list of all the selected cells. For each cell  $s \in S$ , we define the kernel  $K_s \subset S$  as the subset of cells that can be reached by crossing only selected cells and a maximum of  $n$  edges.  $|K_s|$  is the size of the kernel. In the case of the single crack the size of the kernel is always equal to  $2n + 1$ , except for the kernels whose center is close to the boundary of the domain. The kernel size may then be as low as  $n + 1$ . Our method preserves the localization of the deformation ~~by avoiding~~ mixing the deformation between LKFs (i.e., cells where the deformation is intense) and the surrounding rigid plates (i.e., cells where deformation is almost zero). Moreover, the way the smoothing kernels are built ensures that deformation between LKFs that are not connected will not be averaged together.

The proposed method relies on two parameters: the deformation threshold that determines which cells are selected and parameter  $n$  that determines how far we extend the kernel. In our test cases, the threshold value is chosen to be small enough to select all the deforming cells. For application to real data, the choice of this parameter is critical and is detailed in Section 2.2. The impact of parameter  $n$  on the total error, defined as the sum of the opening and closing errors, is shown in Fig. 2 (line with disk symbols). This error, when normalized by the sliding distance  $u_p$ , decreases from about 40% to a residual error that depends on the normalized resolution. For a resolution of 0.1, the residual error ~~is about 10~~ (i.e., the error remaining for  $n > d^{-1}$ ) is about 5% as shown in Fig. 2. Simple analytical developments (not shown here) and numerical experiments with  $d$  ranging [0.1–0.001] show that the residual error for the single slip case is proportional to the normalized resolution, whereas the initial error does not depend on the normalized resolution.

The two other curves in Fig. 2 (with square and triangle symbols) correspond to the normalized errors found for experiments considering a secondary crack as shown in Fig. 3. The domain is now divided in 3 blocks. Points below the principal crack are still fixed. Points above the principal crack ~~experience~~ experiment the same displacement  $u_n$ , perpendicular to the principal crack, but have distinct tangent components  $u_p$  for the block on the left or  $u'_p$  for the block on the right of the secondary crack.

To get one crack opening while the other is closing,  $u'_p$  is defined as  $u_p - u_n$ . The example in Fig. 3 is given for  $u_p = 0.01$  and  $u_n = -0.0025$ , so that the principal crack should be closing whereas the secondary crack should be opening. Before filtering, the computed divergence field is highly polluted by the noise. Once the deformation is filtered (here with  $n = 3$ ), the divergence field better matches the expected opening and closing. At the intersection of the two cracks though, the solution may be incorrect, as the method does not distinguish cracks when they intersect and thus averages deformation over cells belonging to different cracks. It should be also noted that at the intersections of two cracks the size of the kernel  $|K_s|$  may be as high as  $3n + 1$  (for three-branch intersections as in Fig. 3) or  $4n + 1$  (for four-branch intersections).

This mixing of intersecting cracks explains why the normalized error (triangle and square symbols on Fig. 2), after having rapidly decreased for small  $n$  as in the single crack case, starts to increase for larger  $n$ . This simple test case shows that the shape of this function depends on the ratio  $\frac{u_n}{u_p}$  and that the optimal value for  $n$  would be 4 for  $\frac{u_n}{u_p} = \frac{1}{8}$  and 2 for  $\frac{u_n}{u_p} = \frac{1}{4}$ . From this analysis, we identify  $n = 3$  as an optimal value as it is the only value for which the median error is reduced by at least a factor of 3 in any of the test-cases presented here. In real cases, to define an optimal value for  $n$  is more difficult as it would depend on the number of intersecting cracks and on the local ratio between divergence and shear. ~~To optimize~~ For this study, we chose to use a constant parameter  $n$  and its reference value is fixed at  $n = 3$ . To validate the choice of the method ~~parameters,~~ 's parameters (i.e.,  $n$  and the threshold on the total deformation), we present in Sect. 3 another metric based on a ~~multi-fractal~~ multifractal scaling analysis of the deformation fields.

## 2.2 Application to RGPS sea ice trajectories

The RGPS Lagrangian displacement product provides trajectories of sea ice “points” initially located on a 10 km regular grid (<http://rkwok.jpl.nasa.gov/radarsat/lagrangian.html>). The ~~position~~ positions of these points are updated when two successive images are available and treated by the tracking algorithm. The time interval between two updates is typically 3 days. Spatial coordinates are given in the SSM/I polar stereographic projection, with the origin of the Cartesian grid located on the North Pole and the negative  $y$  axis aligned to the 45° W meridian.

The RGPS Lagrangian deformation product provides the deformation of each cell (which is quadrangle) of the original grid. The deformation of a cell is updated each time the position of ~~one of its nodes is~~ all its nodes are updated. This method has ~~two serious problems:~~ first, a serious problem because cells may become so distorted that spatial derivatives are ill-defined ~~and secondly, artificial deformation may arise when only part of the nodes of a cell are updated at the same time~~. As the RGPS deformation dataset does not provide for each cell the position of its node ~~and the date of their last update~~, it is not possible to filter the data to avoid ~~these problems. These problems are~~ this problem. This problem is specific to the RGPS deformation product and would not appear if each pair of images was treated separately with its own grid as in the GlobICE Image Pair product (<http://www.globice.info>) and in the ENVISAT Geophysical Processor System (EGPS) (<http://rkwok.jpl.nasa.gov/envisat/>).

To tackle these problems, we reprocessed the RGPS Lagrangian displacement product to build a new deformation dataset called the RGPS Image Pair Product. We first identify the tracked points corresponding to each pair of images (i.e. the set of points whose position has been updated at the exact same date and with the same time interval). We generate a Delaunay triangulation of these points. Then we compute the deformation over what we consider as being well-shaped cells, i.e. only for triangles having an area between 5 and 400 km<sup>2</sup>, their angles higher than 5° or all their edges shorter than 25 km. We also only keep meshes if they have at least 200 nodes, and we discard single and pairs of triangles that are not connected to other cells. ~~Using triangles instead of quadrangles roughly doubles the~~

~~number of deformation estimates, and increases the resolution of the deformation product up to 7.~~ Figure 4 shows an example of a mesh and a sea ice divergence field after the processing of the data corresponding to one pair of images. Artificial noise, characterized by a succession of highly negative and positive values, is clearly visible and, as expected, is mainly located along lines.

Using triangles instead of quadrangles roughly doubles the number of deformation estimates, and increases the resolution of the deformation product up to 7 km. Another advantage is that triangulations can be made on any set of points (if they are not all aligned), which is not the case with quadrangulation (Bremner et al., 2001) . If the tracked points are given on a regular grid, quadrangulation could be easily performed and could be preferred. However for most of the available datasets (for example GlobICE and EGPS), the data are not given on a grid but as a list of points. The method presented here based on triangles is then very flexible and can be applied to many different sources of data. In the next section, the unfiltered and filtered deformation fields obtained on triangular meshes are compared to the RGPS deformation fields. The smoothing procedure is not applied to the RGPS deformation fields because it requires to know the neighbors of each cell and this information is not present in the RGPS Lagrangian deformation dataset.

To apply the smoother, we first need to detect the cells that are suspected to map the location ~~where of~~ linear kinematic features ~~are~~. Thomas et al. (2008) proposed to use a shear threshold based on the level of noise resulting from the motion tracking error. Instead, here we use a fixed threshold based on the total deformation (as in the simple test case presented above) to give more weight to the cracks suffering from artificial divergence ~~while keeping an important weight for the shear deformation~~. Cells showing total deformation greater than the threshold are thus selected and others simply not taken into account for the filtering procedure. Figure 5 shows the unfiltered total deformation rate and the selected cells (those with their edges in black) for a threshold equal to 0.02 per day.

Decreasing the threshold increases the number of selected cells and finally leads to excessive smoothing. Increasing the threshold reduces the number of selected cells and finally splits linear features into disconnected pieces for which the smoother is not efficient

anymore. Indeed if a kernel only contains one cell, the smoother does not modify the value of the deformation over that cell.

To quantify the effect of this threshold on the quality of the selection, we define an index based on the size of the smoothing kernels. ~~In the case of an isolated crack, the size of the kernel  $|K_s|$  (i.e. the number of cells that can be reached by crossing only selected cells and a maximum of  $n$  edges) is maximum when equal to  $2n + 1$ . It can be as small. As explained in Sect. 2.1, the size of the kernel  $|K_s|$  could be as low as  $n + 1$  if for single cracks when the center of the kernel is at the boundary of the mesh. In the case of and as high as  $4n + 1$  for two intersecting cracks, the maximum size of the kernel increases up to  $4n + 1$ .~~ We then define the quality index as the percentage of treated cells having a kernel size between  $n + 1$  and  $4n + 1$ . For the example of Fig. 5, the quality index is equal to 89 %.

We explored the sensitivity of this quality index to the threshold value for the entire winter season 2006–2007 and with the parameter  $n$  equal to ~~3~~ 3, which is the reference value defined in Sect. 2.1. For deformation thresholds equal to 0, 0.01, 0.02, 0.03, 0.04 and 0.05 per day, median quality indices are equal to 33, 78, 78, 76, 74 and 72 %, respectively. Based on this quality index, the threshold values 0.01 and 0.02 per days are the best. The value of 0.02 per day is chosen as the reference value for the deformation threshold. To quantify the range of the quality index obtained with this reference value, we look at the percentage of pairs of images for the entire winter 2006-2007 for which the quality index is lower than 50 % and we found that only 14 % of the pairs of images have a quality index lower than 50 %. To further validate the choice of the model parameters, a consistency check based on a multifractal scaling analysis of the deformation fields is proposed in Sect. 3.

Figure 6 shows the sea ice divergence field after the application of the smoother with the parameter  $n$  equal to 3. Compared to the unfiltered divergence field shown in Fig. 4, the filtered field exhibits much less artificial noise and its interpretation is now much easier.

### 3 Results and discussion

In this section, we compare the original RGPS deformation data to the unfiltered and filtered versions of our RGPS Image Pair dataset. A ~~validation metric consistency check~~ based on spatial scaling analysis is proposed and the differences between the three datasets in terms of spatial scaling and total opening/closing are discussed.

To compare the original RGPS deformation data with the unfiltered and filtered deformation data produced by our method, we generate composite pictures of the deformation rates for specific periods. The periods have to be ~~large long~~ enough to ensure a good spatial coverage, but not too ~~large long~~ to avoid mixing incoherent information. For this study, we select the data for which the time of the first and second images, noted  $t_{k-1}$  and  $t_k$  respectively, are within a period of 8 days centered on a target date, and for which the time interval,  $\Delta t = t_k - t_{k-1}$ , is between 1 and 6 days. For the RGPS dataset, we add a criterion to reject cells larger than 400 km<sup>2</sup>.

Selected cells may cover the same area but correspond to different dates and time intervals. This redundancy may impact statistical distribution and scaling analysis, so we apply a second selection step. We first define a regular grid at a resolution of 20 km. For each box of this grid, we find the cells whose center is in the box and we keep only those whose date, defined as  $(t_k + t_{k-1})/2$ , is the closest to the target date. This selection step creates some gaps in the coverage but is necessary to ensure a minimum consistency of the composite fields. Note that no averaging or interpolation is done during the generation of the composite deformation fields.

Figure 7 shows the divergence rate for the period 2–10 February 2007 given by the RGPS Lagrangian deformation dataset. Some features are so polluted by a succession of highly negative and positive values that it is very difficult to identify ~~which where~~ cracks are opening, closing or sliding. Figure 8 shows the unfiltered divergence rate for the same period obtained after the first step of our method. As in the RGPS dataset, the artificial noise is important and mainly located along linear kinematic features. Figure 9 shows the filtered divergence rate obtained with a deformation threshold of 0.02 per day and  $n = 3$ .

The reduction of the noise makes much easier the identification of the opening and closing cracks.

### 3.1 ~~Validation~~Consistency check

To ~~validate~~evaluate our method in a more quantitative way, we propose a metric based on a spatial scaling analysis. Scaling analysis is a powerful tool to characterize sea ice dynamical behavior, and has been successfully used in previous studies to reveal the power-law scaling of sea ice deformations (Marsan et al., 2004; Rampal et al., 2008). ~~Since the result of the scaling analysis is by definition very sensitive to the presence of noise and extreme values in the analyzed field, one may use it to check the presence of spurious noise in deformation datasets.~~

The spurious noise in the deformation fields corresponds to high values of deformation and is potentially present for any active linear kinematic features. This noise may then impact the distributions of shear and absolute divergence and modify their mean (1<sup>st</sup>-order moment) but even more their standard deviation (2<sup>nd</sup>-order moment) and skewness (3<sup>rd</sup>-order moment). Moreover this noise is the highest at the resolution of the data but rapidly decreases for larger spatial scales. We then expect that the presence of noise in the deformation fields will have a strong impact on the result of the scaling analysis, especially for the smallest scales and the highest-order moments of the distribution. Indeed, we assume that the power-law model for the spatial scaling of sea ice deformations has no physical reason to not hold over several orders of magnitude. This assumption is based on Weiss and Marsan (2004) who showed that the power-law model for the spatial scaling of the open water density, which can be directly related to sea ice divergence, is valid down to 0.2 km. Therefore, any significant departure from the power-law model when approaching the spatial resolution of the data ~~can~~could be seen as an indicator of the remaining noise in the deformation field.

To perform the scaling analysis of sea ice deformation, we implemented a coarse graining method similar to the one proposed by Marsan et al. (2004) and applied it to the unfiltered and filtered versions of our RGPS Image Pair dataset. Sea ice shear and absolute diver-

gence rates are computed at different spatial scales ranging from 7 to 700 km. ~~The values obtained for each scale~~ For the lowest scale, which is also the scale of the triangular cells, all the cells are taken into account. For the other scales, the coarse graining procedure covers the domain with boxes of different sizes (14, 28, 56, 112, 224, 448 and 896 km). The boxes actually overlap each other since a distance equal to half the box size separates their respective centers. For each box, we select the cells that have their center in the box. When the sum of the area of those cells is greater than half the box area, the deformation over the box is defined by averaging the spatial derivatives of the displacement weighted by the surface of each cell. The spatial scale for this new estimate of the deformation is the square root of the sum of the cell areas. The shear and absolute divergence for each box are then reported as a function of the spatial scale on a log-log plot (see Fig. 10 for the absolute divergence rate). The mean value  $\langle \dot{\epsilon}_L \rangle$  (where  $\dot{\epsilon}_L$  is either the shear rates or the absolute divergence rates, computed at scale  $L$ ) relates to scale  $L$  following a power law. The power-law exponent is evaluated by applying a linear regression of the logarithm of  $\langle \dot{\epsilon}_L \rangle$  vs. the logarithm of  $L$ . Due to the finite size of the domain the power-law model is not expected to hold for the largest scales. For this reason we restrict the power-law regression of the data to the spatial scales 7, 14, 25, 50, 100 and 200 km.

The ~~artificial noise particularly induces a strong departure from filtered shear and absolute divergence closely follows~~ the power-law model ~~at the smallest scales (see for the spatial scaling as their first order moments are well aligned with the power-law fit for the spatial scales ranging from 7 to 200 km (see right panel of Fig. 10 )~~ for the absolute divergence). This is not the case for the unfiltered deformation fields (see left panel of Fig. 10) and we explain this strong departure from the power-law model by the presence of artificial noise. If the power-law fits were computed only from 50 to 200 km, spatial scaling exponents would be similar for the filtered and unfiltered data. Furthermore, the other moments  $\langle \dot{\epsilon}_L^q \rangle$  of the distributions (see Fig. 11, for the absolute divergence rate, with  $q$ , the moment order, ranging from 0.5 to 3) computed from the unfiltered deformation fields also exhibit a strong departure from the power law, whereas the moments computed from the filtered deformation fields are well aligned with the power-law fits.

~~The method parameters are then chosen to minimize~~ By definition, if a scaling holds for a given range of scales, it should be respected for any pair of scales within this range. To evaluate the deviation from the power law ~~. To evaluate this deviation~~ scaling, we compute the power-law exponents for each pair of successive spatial scales (i.e. from 7 to 14 km, from 14 to 25 km, and so on) and we take the minimum and maximum values of these exponents ~~to define the min-max error on the~~. Those values as well as the exponents previously obtained ~~(i.e. with the whole range from 7 to 200 km)~~ are reported as a function of the moment order  $q$  in Fig. 12. The relationship between the power-law exponents and the moment order  $q$  is called the structure function  $\beta(q)$  and is defined by  $\langle \dot{\epsilon}_L^q \rangle \sim L^{-\beta(q)}$ . The minimum and maximum exponents define the bars around  $\beta(q)$ .

To check that the reference values for the model parameters are well chosen, we look at the deviation from the power law. This deviation is evaluated by the min-max error. For each moment order, the min-max error is defined as the difference between the minimum and maximum exponents obtained with any pairs of spatial scales within the defined range. In other words, it is the length of the bar drawn on Fig. 12. Applied to the composite fields used as example here, ~~this metric validates the choice of using  $n = 3$  and we find that using~~ a threshold for the total deformation of 0.02 per day ~~, as this combination~~ gives the lowest min-max ~~errors~~ error for the highest order. For the parameter  $n$ , the lowest min-max error for the highest moment order is obtained with  $n = 2$ , but  $n = 3$  is better for the other moment orders. The application of our metric to this single example tends to indicate that the reference values are well chosen. However, this metric should be applied to a larger number of examples to really identify the best values for the parameters.

### 3.2 Discussion

Comparing the original RGPS deformation to the unfiltered deformation allows us to evaluate the impact of using a triangulation to define well-shaped triangular cells. As in Lindsay and Stern (2003), we observe unrealistic values for the shear and divergence rates retrieved from the RGPS deformation dataset. For the period 2–10 February 2007, the composite picture made from RGPS has maximum opening, closing and shear rates equal to 1.73,  $-6.73$

and 66.47 per day, respectively. These extreme values arise from highly distorted cells ~~or from cells with inconsistent updates for the positions of their nodes~~. A very small fraction of the dataset is polluted by these unrealistic values, however it has a high impact on the multifractal scaling analysis, particularly when looking at the highest moment orders of the distributions. In Marsan et al. (2004) and Stern and Lindsay (2009), additional constraints on the initial and current size of the cells were applied and the cells with total deformation higher than 1 per day were not taken into account. In many other studies based on the RGPS deformation dataset, the presence and impacts of these unrealistic extreme values are simply not discussed.

The simple fact of redefining a new mesh from the actual position of the RGPS nodes allows us to avoid badly shaped cells and then to significantly reduce the number and magnitude of extreme values. For the same period, the composite picture obtained from the unfiltered version of our RGPS Image Pair dataset has maximum opening, closing and shear rates equal to 0.63,  $-1.17$  and  $1.97$  per day, respectively. The smoother also logically decreases the extreme values. For this example, the filtered composite picture has maximum opening, closing and shear rates equal to  $0.13$ ,  $-0.20$  and  $0.73$  per day, respectively.

Comparing the filtered and unfiltered deformation allows us to analyze the impact of the artificial noise. From the scaling analysis for the total deformation, shear and absolute divergence, we found that the scaling exponents estimated from the unfiltered fields are systematically ~~higher~~ larger in magnitude by about 100 % for the absolute divergence and by about 50 % for the shear and total deformation. In the example corresponding to Fig. 10, the power-law exponent for the absolute divergence is  $-0.38$  for the unfiltered field, instead of  $-0.20$  for filtered data (for the shear:  $-0.17$  instead of  $-0.1$ , and for the total deformation:  $-0.19$  instead of  $-0.12$ ). For each moment, we observe that using unfiltered data leads to a systematic overestimation of the scaling exponents of about 100 % for the absolute divergence and 50 % for the shear and total deformation. We also performed the multifractal scaling analysis on the original RGPS deformation dataset with the same constraints on the data as in Stern and Lindsay (2009) and we found that the departure from the power-law is similar to the one observed for the unfiltered deformation data set.

The impact of the artificial noise ~~may also be illustrated by~~ is also seen on the structure function  $\beta(q)$  ~~which is defined by  $\langle \dot{\epsilon}_L^q \rangle \sim L^{-\beta(q)}$  (see Fig. 12). The bars around  $\beta(q)$  correspond to the min-max errors used for the validation.~~ As a consequence of the systematic overestimation of the scaling exponents, ~~the curvature of  $\beta(q)$~~  its curvature, which indicates the degree of multifractality of the deformation fields, is found twice as high for the unfiltered divergence field (0.20) than for the filtered one (0.11). For the shear and total deformation, the overestimation of the curvature is about 50 %, with a value of 0.16 instead of 0.1.

Differences are also seen in the cumulative distribution of the closing and opening rates (see Fig. 13, for the period 2–10 February 2007). Differences between the RGPS and the unfiltered deformation may be due to differences in the coverage and the selection of the data, but also come from the difference in resolution (10 km for the RGPS instead of 7 km) and from the impact of distorted cells included in the RGPS dataset. Differences between the filtered and unfiltered deformation induce a modification of the shape of the distribution. The distribution of the filtered divergence field is closer to an exponential distribution (linear in the semi-log plot), while the distribution of the unfiltered divergence field is clearly a stretched exponential.

Finally, we compare the three datasets by computing the total area that has been opened and closed. For the original RGPS deformation data, 40 000 km<sup>2</sup> have been opened during the period 2–10 February 2007, whereas 39 000 km<sup>2</sup> have been closed. For our unfiltered data, we find lower values of 30 000 and 38 000 km<sup>2</sup>, respectively. For the filtered data these numbers drastically ~~drops~~ drop down to 15 000 and 24 000 km<sup>2</sup>, respectively. In this example the artificial noise is then responsible of an overestimation of the opening and closing of about 100 and 60 %, respectively. Over the entire winter season 2006–2007, the ~~cumulated~~ cumulative opening and closing are both 60 % higher in the unfiltered data than in the filtered data.

## 4 Conclusions

A method is proposed to derive accurate sea ice deformation fields from SAR-derived motion products. The first step of the method consists of a triangulation of the tracked points to generate a mesh of triangular cells on which a first estimate of deformation is computed. The second step consists of applying a smoother to the deformation fields. The method relies on two parameters: a deformation threshold and the size of the smoothing kernel.

By applying the method to ~~simple test cases and to real data, optimal values for the method parameters are proposed.~~ The idealized test cases, we show that using triangles instead of quadrangles induces an increase of about 10 % of the opening and closing error, whereas our smoothing method reduces the opening and closing error by at least a factor of 3 in any of the test-cases presented here. The sensitivity to the value of the threshold used to detect deformation features is analyzed with a quality index and the efficiency of our method is assessed using a metric based on a spatial scaling analysis and comparison between the unfiltered and filtered deformation fields.

The proposed method is used to produce a new deformation dataset called RGPS Image Pair Product. Compared to the RGPS deformation dataset, the RGPS Image Pair dataset does not exhibit unrealistic large values caused by badly shaped cells ~~or inconsistent updates of the cell node position~~. Moreover, our method drastically reduces the artificial noise arising along dynamic discontinuities.

By comparing the unfiltered and filtered deformation fields for winter 2006–2007, we estimate that this artificial noise may cause an overestimation of the opening and closing of about 60 %. We also estimate that the spatial scaling exponents as computed in Marsan et al. (2004) and Stern and Lindsay (2009) could have been overestimated by about 100 % for the absolute divergence and by about 60 % for the shear and total deformation.

The findings of the present study indicate that errors in sea ice deformation fields retrieved from SAR-derived motion may have been strongly underestimated, leading to potential significant biases on the estimates of sea ice production, salt rejection and sea ice ridging that one may find in the literature.

The method proposed here is applicable to other sea ice drift datasets, as provided, for example, by GlobICE project. The method can handle Lagrangian trajectories or displacement between pairs of images. The same method could be applied to [buoys-buoy](#) trajectories when their spatial resolution is high enough, as with nested arrays of buoys (Hutchings et al., 2011, 2012).

The method proposed here could be modified to better manage intersecting cracks and to adapt its parameters depending on the local fields. However, substantial improvements may also come by combining within tracking algorithms, the detection of dynamic discontinuities and the computation of sea ice deformation as proposed by Thomas et al. (2008). [A complete validation using independent datasets should also be done.](#)

*Acknowledgements.* Sylvain Bouillon is supported by the Research Council of Norway through the post-doc project SIMech, Sea Ice Mechanics: from satellites to numerical models (No. 231179/F20, 2014–2016). Pierre Rampal is supported by the Kara Sea project sponsored by Total E&P. Many thanks to Tim Williams and Gunnar Spreen for interesting discussions.

## References

- [Bremner, D., Hurtado, F., Ramaswami, S., and Sacristán, V.: Small convex quadrangulations of point sets, in: Algorithms and Computation, edited by Eades, P. and Takaoka, T., vol. 2223 of Lecture Notes in Computer Science, pp. 623–635, Springer Berlin Heidelberg, doi:10.1007/3-540-45678-3\\_53, 2001.](#)
- [Fily, M., and Rothrock, D.: Opening and closing of sea ice leads: digital measurements from synthetic aperture radar, J. Geophys. Res., 95, 789–796, doi:10.1029/JC095iC01p00789, 1990.](#)
- Girard, L., Weiss, J., Molines, J.-M., Barnier, B., and Bouillon, S.: Evaluation of high-resolution sea ice models on the basis of statistical and scaling properties of Arctic sea ice drift and deformation, J. Geophys. Res., 114, 2156–2202, doi:10.1029/2008JC005182, 2009.
- Girard, L., Bouillon, S., Weiss, J., Amitrano, D., Fichet, T., and Legat, V.: A new modelling framework for sea ice mechanics based on elasto-brittle rheology, Ann. Glaciol., 52, 123–132, 2011.
- Herman, A. and Glowacki, O.: Variability of sea ice deformation rates in the Arctic and their relationship with basin-scale wind forcing, The Cryosphere, 6, 1553–1559, doi:10.5194/tc-6-1553-2012, 2012.

- Hollands, T. and Dierking, W.: Performance of a multiscale correlation algorithm for the estimation of sea-ice drift from SAR images: initial results, *Ann. Glaciol.*, 52, 311–317, doi:10.3189/172756411795931462, 2011.
- Hutchings, J. K., Roberts, A., Geiger, C. A., and Richter-Menge, J.: Spatial and temporal characterization of sea-ice deformation, *Ann. Glaciol.*, 52, 360–368, 2011.
- Hutchings, J. K., Heil, P., Steer, A., and Hibler III, W. D.: Subsynoptic scale spatial variability of sea ice deformation in the western Weddell Sea during early summer, *J. Geophys. Res.*, 117, C01002, doi:10.1029/2011JC006961, 2012.
- [Kwok, R.: The RADARSAT Geophysical Processor System. in Analysis of SAR data of the Polar Oceans: Recent Advances, Tsatsoulis, C. and R. Kwok, Eds.: 235-257, Springer Verlag, 1998](#)
- Kwok, R.: Contrasts in sea ice deformation and production in the Arctic seasonal and perennial ice zones, *J. Geophys. Res.*, 111, C11S22, doi:10.1029/2005JC003246, 2006.
- Kwok, R. and Cunningham, G. F.: Seasonal ice area and volume production of the Arctic Ocean: November 1996 through April 1997, *J. Geophys. Res.*, 107, 8038, doi:10.1029/2000JC000469, 2002.
- Kwok, R. and ~~Rothrock, D. A.~~, Stern, H. L., and [Cunningham, G. F.](#): Determination of the age distribution of sea ice from Lagrangian observations of ice motion, *IEEE T. Geosci. Remote*, 33, 392–400, 1995.
- Kwok, R., ~~Schweiger, A., Rothrock, D., Curlander, J. C., McConnell, R., and Pang, S. S., and Kottmeier, C.~~: [Sea ice motion from satellite passive microwave imagery assessed with ERS SAR and buoy motions, J. Geophys. Res., 103, 8191–8214, 1998.](#) [An Ice Motion Tracking System at the Alaska SAR Facility, IEEE J. of Oceanic Engineering, 15, 44–54, 1990.](#)
- Kwok, R., Hunke, E. C., Maslowski, W., Menemenlis, D., and Zhang, J.: Variability of sea ice simulations assessed with RGPS kinematics, *J. Geophys. Res.*, 113, 2156–2202, doi:10.1029/2008JC004783, 2008.
- Lindsay, R. W. and Stern, H. L.: The RADARSAT geophysical processor system: quality of sea ice trajectory and deformation estimates, *J. Atmos. Ocean. Tech.*, 20, 1333–1347, 2003.
- Lindsay, R. W., Zhang, J., and Rothrock, D. ~~a~~A.: Sea-ice deformation rates from satellite measurements and in a model, *Atmos. Ocean*, 41, 35–47, doi:10.3137/ao.410103, 2003.
- Marsan, D., Stern, H. L., Lindsay, R., and Weiss, J.: Scale dependence and localization of the deformation of Arctic sea ice, *Phys. Rev. Lett.*, 93, 178501–178504, doi:10.1103/PhysRevLett.93.178501, 2004.

- Rampal, P., Weiss, J., Marsan, D., Lindsay, R., and Stern, H. L.: Scaling properties of sea ice deformation from buoy dispersion analysis, *J. Geophys. Res.*, 113, C03002, doi:10.1029/2007JC004143, 2008.
- Stern, H. L. and Lindsay, R.: Spatial scaling of Arctic sea ice deformation, *J. Geophys. Res.*, 114, C10017, doi:10.1029/2009JC005380, 2009.
- Thomas, M., Geiger, C. A., and Kambhamettu, C.: High resolution (400 m) motion characterization of sea ice using ERS-1 SAR imagery, *Cold Reg. Sci. Technol.*, 52, 207–223, doi:10.1016/j.coldregions.2007.06.006, 2008.
- [Thorndike, A. S.: Kinematics of Sea Ice, in \*The Geophysics of Sea Ice, NATO ASI Series\*, edited by N. Untersteiner, Plenum Press, New York, 489–549, 1978.](#)
- Weiss, J. and Marsan, D.: Scale properties of sea ice deformation and fracturing, *C. R. Phys.*, 5, 735–751, 2004.

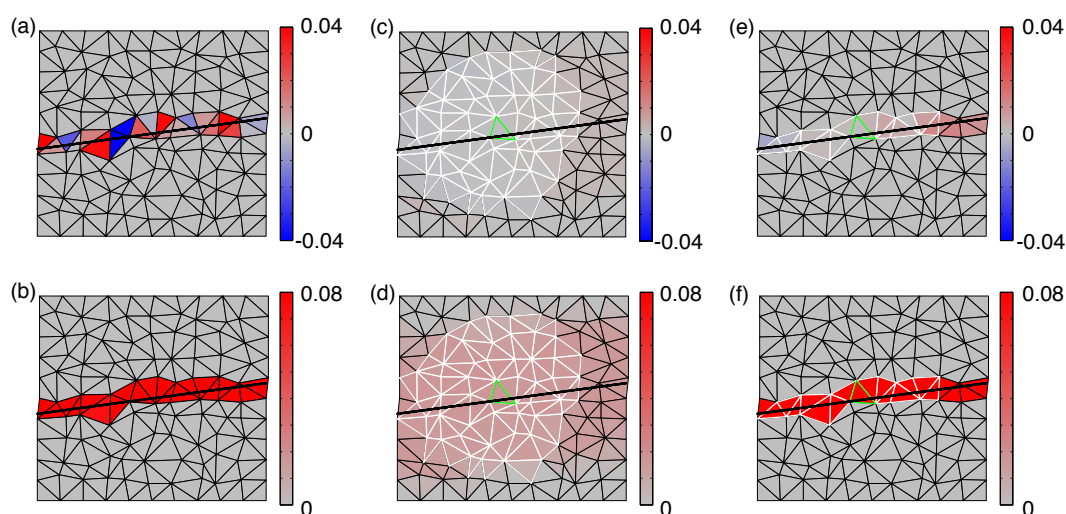


**Figure 1.** Example of the divergence (**a**, **c**, **e**) and shear (**b**, **d**, **f**) obtained for the single crack test case at a [normalized](#) resolution of 0.1. The relative displacement parallel and normal to the crack (black line) are set to 0.01 and 0, respectively. (**a**) and (**b**) correspond to the unfiltered deformation fields, (**c**) and (**d**) to the deformation fields filtered with a classical smoothing kernel and (**e**) and (**f**) to the deformation fields filtered with our smoother. Triangles in white show the kernel defined for the triangle in green. With both smoothers the kernel corresponds to cells that can be reached by crossing a maximum of  $n$  edges (here  $n = 7$ ). The classical smoother takes all the cells into account whereas our smoother only takes into account the cells whose deformation is above a given threshold.

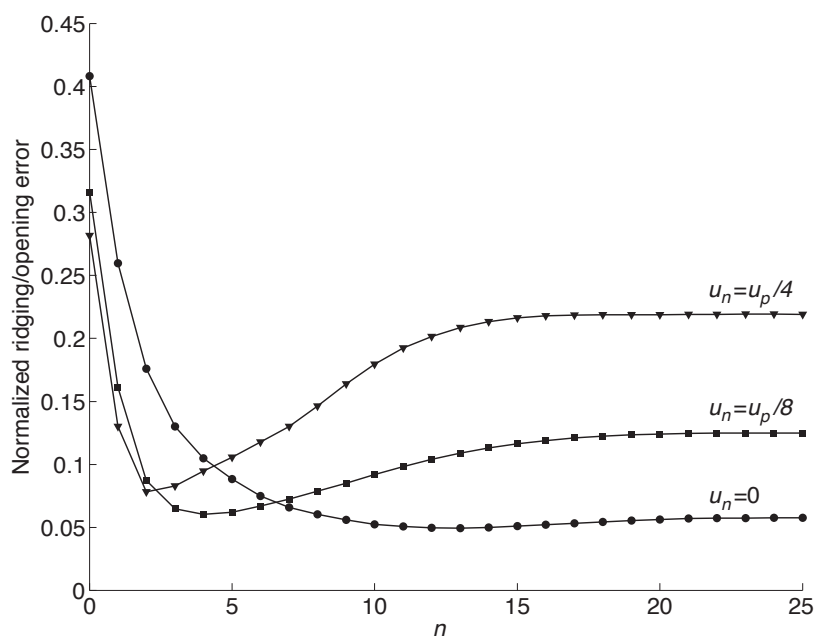


**Figure 2.** Root mean square ridgingclosing/opening error normalized by  $u_p$  and computed from 100 realizations of the single crack (discs) and double cracks test cases (squares and triangles) at the resolution 0.1. For all curves,  $u_p = 0.01$ .

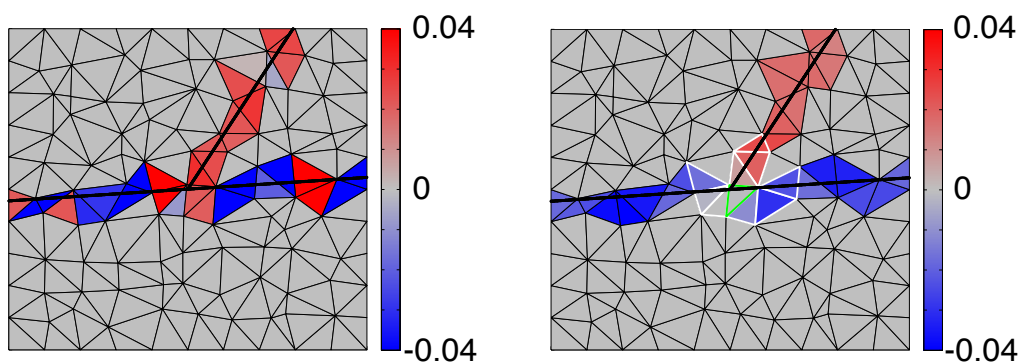


**Figure 3.** Example of the unfiltered (left panel) and filtered (right panel) divergence obtained for the double cracks test case at a normalized resolution of 0.1. The domain is divided in 3 blocks. Points below the principal crack are fixed. Points above the principal crack ~~experience~~ experiment the same displacement  $u_n$ , perpendicular to the principal crack (here  $u_n = -0.0025$ ) but have distinct tangent components,  $u_p$  for the block on the left (here  $u_p = 0.01$ ) and  $u'_p$  for the block on the right of the secondary crack (here  $u'_p = 0.0125$ ). Triangles in white show the kernel defined for the triangle in green. In this example, the parameter  $n$  is equal to 3.

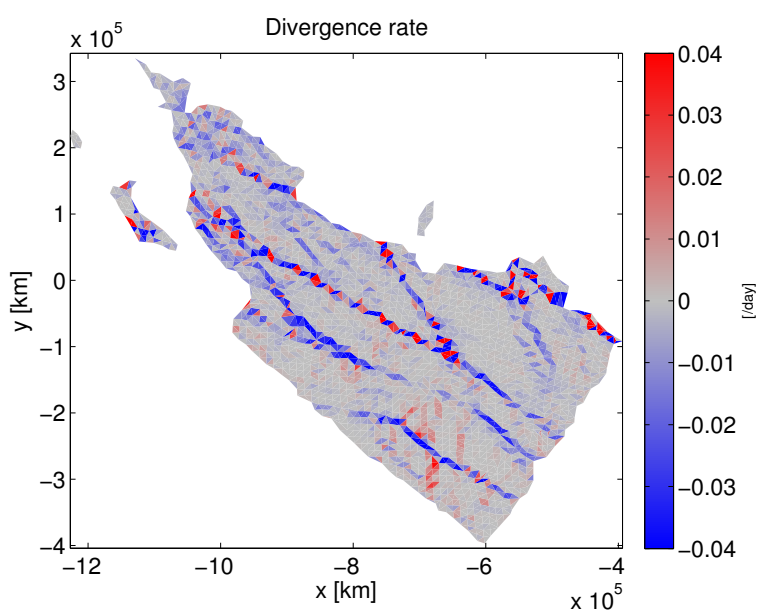


**Figure 4.** Unfiltered divergence rate computed from the RGPS sea ice trajectory dataset and corresponding to the pair of images taken at  $t_{k-1} = 3$  February 2007 17:44:00 UTC and  $t_k = 7$  February 2007 17:26:35 UTC.

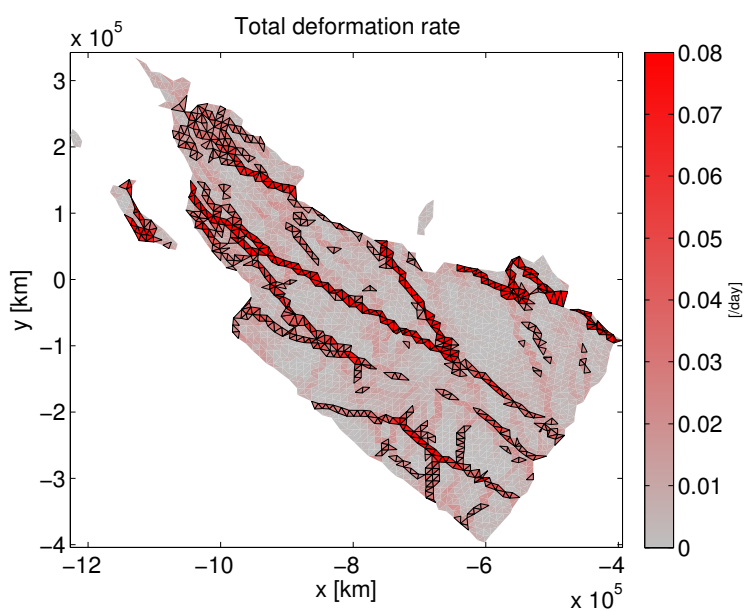


**Figure 5.** Unfiltered total deformation rate for the same example as in Fig. 4. Triangles in black are above the threshold for the total deformation (here, 0.02 per day) and are then selected to be treated by the smoother.

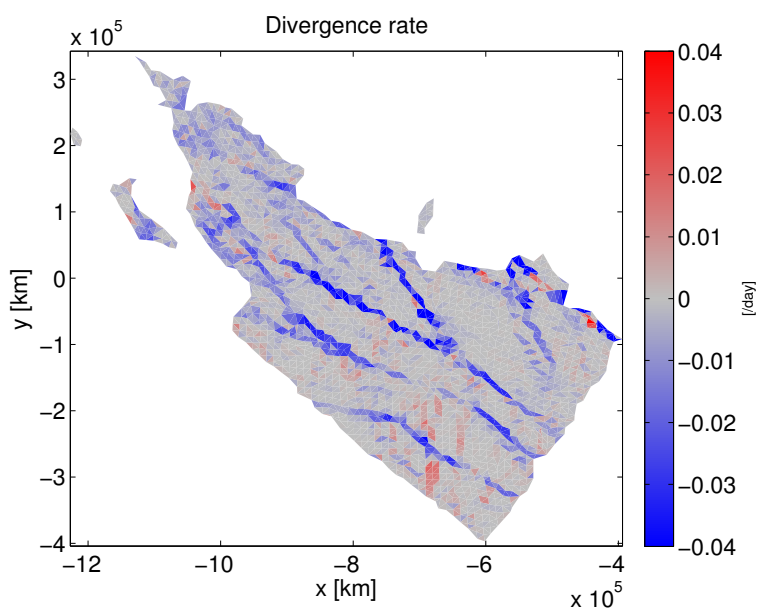


**Figure 6.** Filtered divergence rate after the application of the smoother to the selected cells (see Fig. 5). In this example, the parameter  $n$  is set to 3. The triangles that have been treated by the smoother are those in black in Fig. 5. For the other triangles, the value of the deformation remains the same as in Fig. 4.

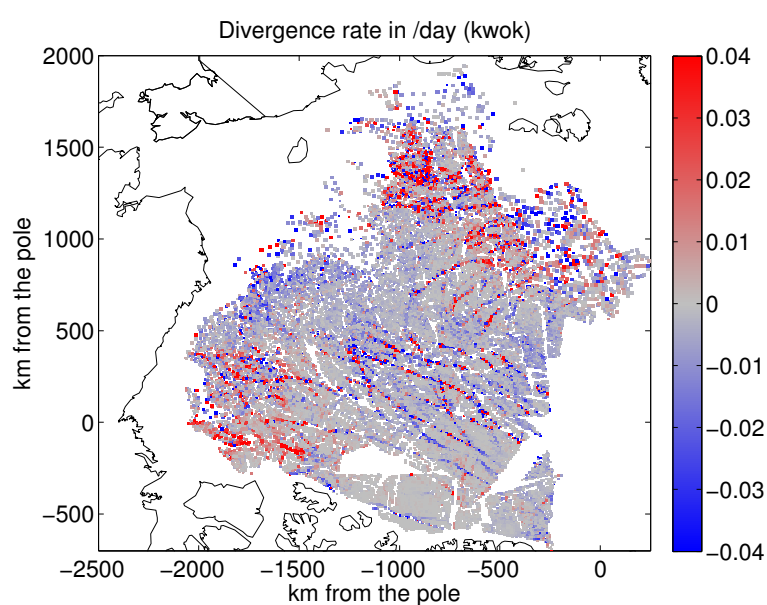


**Figure 7.** Composite picture of the divergence rate given by the RGPS deformation dataset for the period 2–10 February 2007. RGPS cells are here represented by squares as their actual shape is not known.

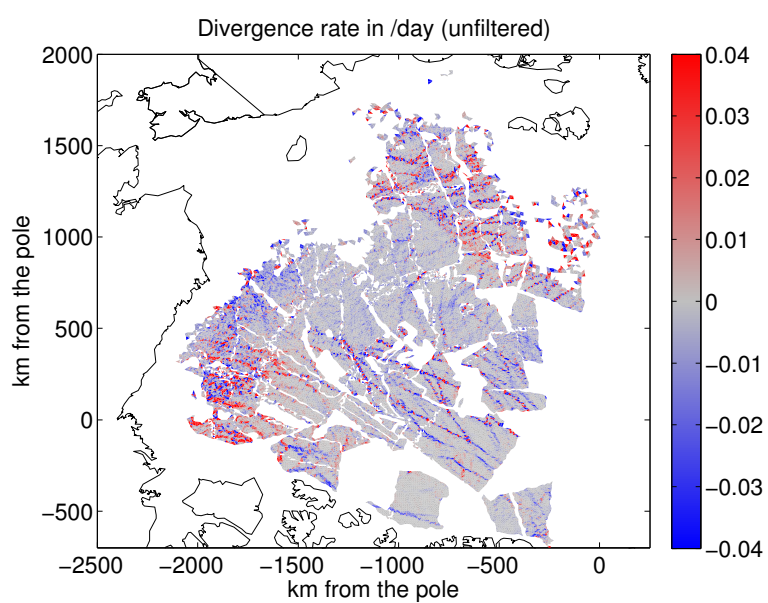


**Figure 8.** Composite picture of the unfiltered divergence rate computed after the first step of our method for the period 2–10 February 2007.

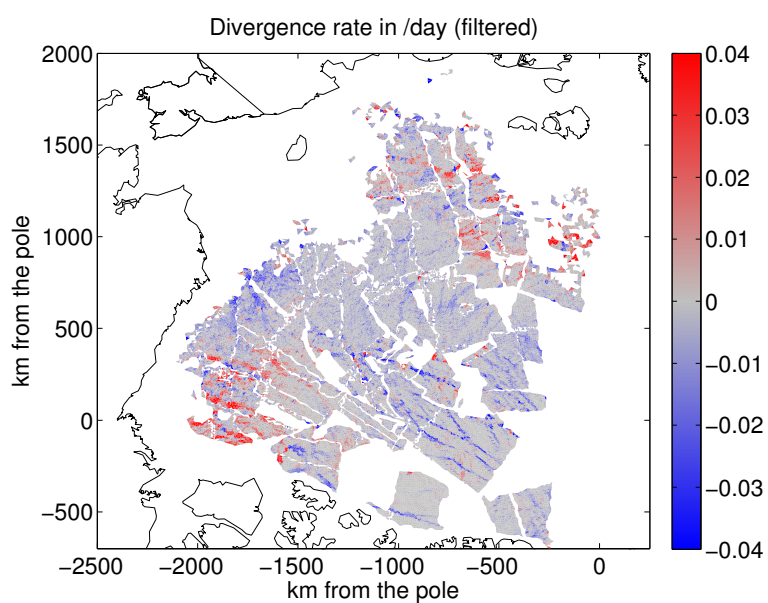


**Figure 9.** Composite picture of the filtered divergence rate for the period 2–10 February 2007 obtained with a threshold parameter equal to 0.02 per day and with the parameter  $n$  equal to 3.

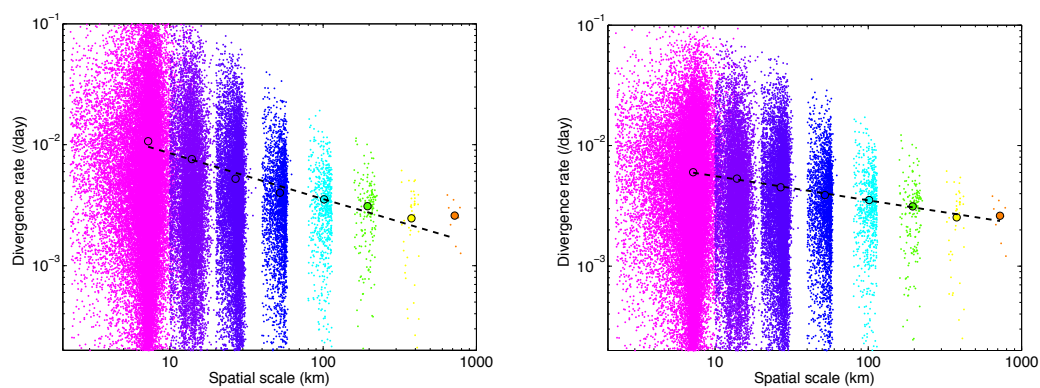


**Figure 10.** Scaling analysis: absolute divergence rate as a function of the spatial scale, from the unfiltered (left panel) and filtered (right panel) composite deformation field for the period 2–10 February 2007–2007 (each color corresponds to a different box size used for the coarse graining procedure). The mean values  $\langle |\dot{\epsilon}_n| \rangle$  and  $\langle |\dot{\epsilon}_{div}| \rangle$  are represented by circles and the dashed lines are power-law fits of the first six mean values (here, from 7 to 200 km)

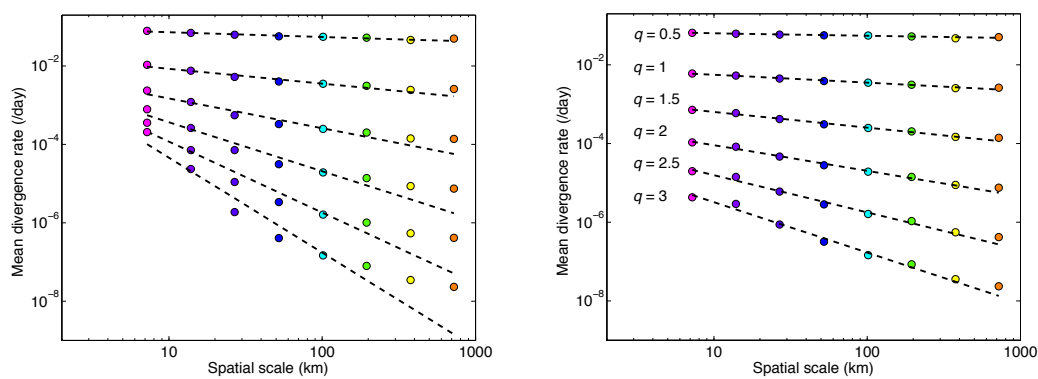


**Figure 11.** Multi-fractal analysis: moments of the absolute divergence rates  $\langle |\dot{\epsilon}_n|^q \rangle$  as a function of the scale  $L$  for  $q = 0.5$  to 3, from the unfiltered (left panel) and filtered (right panel) composite deformation field for the period 2–10 February 2007. Dashed lines are power-law fits of the first six values (here, from 7 to 200 km).

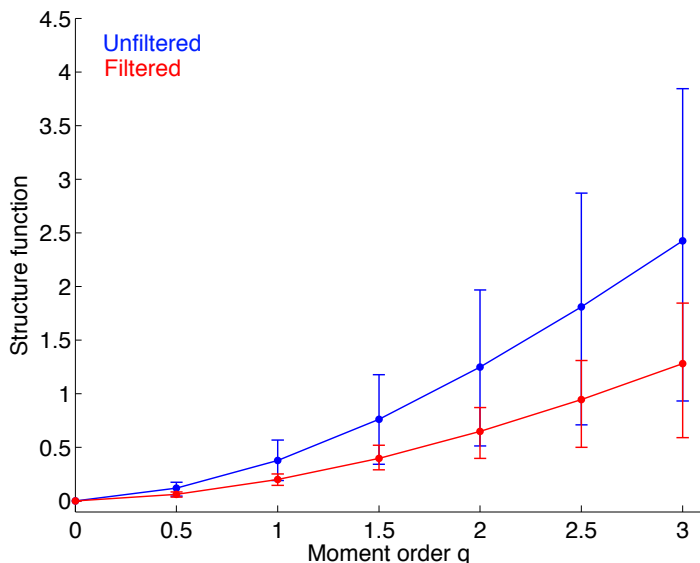


**Figure 12.** Structure function  $\beta(q)$  corresponding to the exponents of the power-law relationship between the absolute divergence rate and the spatial scale:  $\langle |\dot{\epsilon}_n|^q \rangle \sim L^{-\beta(q)}$ ,  $\langle |\dot{\epsilon}_{div}|^q \rangle \sim L^{-\beta(q)}$ . The bars on the graph indicate the deviation from the power law as they correspond to the minimum and maximum power-law exponents obtained for two successive spatial scales.

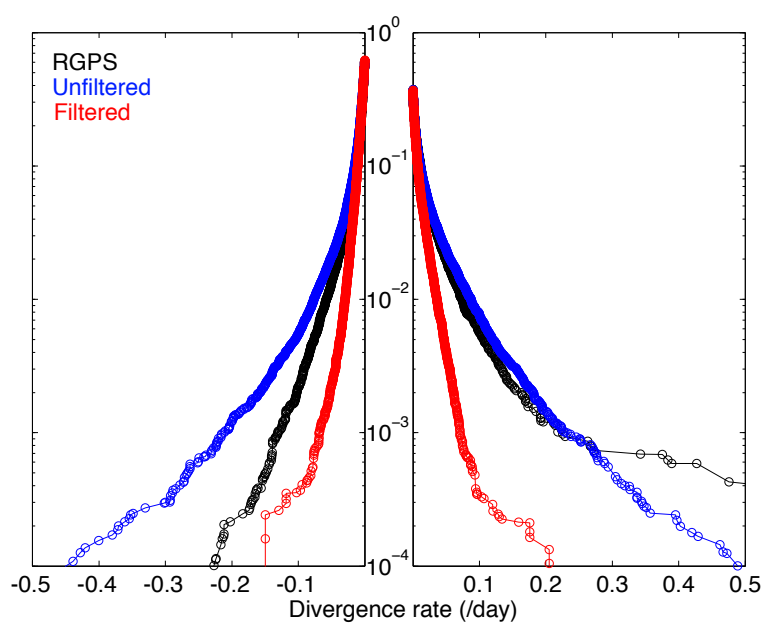


**Figure 13.** Cumulative probability functions, in other words the probabilities of exceedance, for the RGPS, unfiltered and filtered composite divergence fields shown in Figs. 7–9, respectively.